npj | vaccines

Article

Published in partnership with the Sealy Institute for Vaccine Sciences

https://doi.org/10.1038/s41541-024-00992-z

High protection and transmission-blocking immunity elicited by single-cycle SARS-CoV-2 vaccine in hamsters

Martin Joseph Lett[1,6], Fabian Otte[1,6], David Hauser[1,6], Jacob Schön[2], Enja Tatjana Kipfer[1], Donata Hoffmann[2], Nico J. Halwe[2], Angele Breithaupt[3], Lorenz Ulrich[2], Tobias Britzke[3], Jana Kochmann[4], Björn Corleis[4], Yuepeng Zhang[1], Lorena Urda[1], Vladimir Cmiljanovic[5], Christopher Lang[1], Martin Beer[2], Christian Mittelholzer[1,5,7] & Thomas Klimkait[1,7] ✉

Vaccines have played a central role in combating the COVID-19 pandemic, but newly emerging SARS-CoV-2 variants are increasingly evading first-generation vaccine protection. To address this challenge, we designed "single-cycle infection SARS-CoV-2 viruses" (SCVs) that lack essential viral genes, possess distinctive immune-modulatory features, and exhibit an excellent safety profile in the Syrian hamster model. Animals intranasally vaccinated with an Envelope-gene-deleted vaccine candidate were fully protected against an autologous challenge with the SARS-CoV-2 virus through systemic and mucosal humoral immune responses. Additionally, the deletion of immune-downregulating viral genes in the vaccine construct prevented challenge virus transmission to contact animals. Moreover, vaccinated animals displayed neither tissue inflammation nor lung damage. Consequently, SCVs hold promising potential to induce potent protection against COVID-19, surpassing the immunity conferred by natural infection, as demonstrated in human immune cells.

Since its first appearance in 2019, SARS-CoV-2 has spread rapidly worldwide and continues to circulate in many countries, causing symptoms and COVID-19 disease, despite an unprecedented, swift deployment of effective first-generation mRNA- and vector-based vaccines[1–5] that target the viral Spike (S) protein. Since then, multiple virus variants have emerged, carrying escape mutations mainly in the S gene, which correlate with declining protection rates[6,7].

To combat new variants of the virus and induce a broad immune response to more viral proteins, promising recent vaccine approaches focus on attenuating the virus[8–10] and favoring the intranasal route to induce stronger mucosal immunity[11]. However, these recent approaches have not succeeded in inducing transmission-blocking immunity[9,10]. Principal drawbacks of attenuation include residual infectivity or the risk of spontaneous reversion to virulence, i.e., causing the *wild-type* disease from which one would like to protect[12,13]. This is particularly crucial for at-risk groups such as immunocompromised, transplanted, and elderly individuals or cancer patients.

To generate a safe and effective next-generation SARS-CoV-2 vaccine that induces a potent immune response, we developed the 'single-cycle infection concept'. By deleting the essential structural Envelope (E) gene from the viral genome and combining it with a stable cellular trans-complementation system, as described for other coronaviruses[14–17], we produced an intact but propagation-defective vaccine virus to serve as a SARS-CoV-2 vaccine candidate.

E, the smallest essential structural viral gene involved in viral budding, was selected to render the vaccine virus single-cycle. With its small size, it is also well-suited for manipulation due to its minimal genetic burden. Additionally, the E gene encodes a low-abundance, membrane-embedded viroporin that is poorly immunogenic and contributes insignificantly to T-cell responses[18,19]. For better traceability during initial research, the E gene was replaced with an eGFP reporter (ΔE^G).

To simultaneously enhance immune functions, we deleted critical accessory genes: open reading frame 6 (ORF6) has been described to suppress the T cell response[20] and eliminate the interferon (IFN) response in the infected cells[21]. ORF8 has been shown to reduce the T-cell response in vivo[22,23]. Moreover, ORF6 and ORF8 are non-structural cytoplasmic proteins that will not have a major impact on antibody responses to the virus.

[1]Molecular Virology, Department of Biomedicine, University of Basel, Basel, Switzerland. [2]Institute of Diagnostic Virology, Friedrich-Loeffler-Institute, Greifswald - Isle of Riems, Greifswald, Germany. [3]Department of Experimental Animal Facilities and Biorisk Management, Friedrich-Loeffler-Institute, Greifswald - Isle of Riems, Greifswald, Germany. [4]Institute of Immunology, Friedrich-Loeffler-Institute, Greifswald – Isle of Riems, Greifswald, Germany. [5]RocketVax AG, Basel, Switzerland. [6]These authors contributed equally: Martin Joseph Lett, Fabian Otte, David Hauser [7]These authors jointly supervised this work: Christian Mittelholzer, Thomas Klimkait. ✉e-mail: thomas.klimkait@unibas.ch

The elimination of ORF6 and ORF8 is thereby expected to increase the immunogenicity of single-cycle infection viruses (SCVs) beyond that of a natural SARS-CoV-2 infection while reinforcing the high level of safety[24,25].

This study investigates the properties of a single-cycle, triple-deletion vaccine virus (ΔE^G68) and assesses the direct impact of eliminating ORF6 and ORF8 by comparing it to an "E-deleted only" virus (ΔE^G). We show evidence of enhanced immune stimulation, the elicitation of full protection against challenge infection, and transmission-blocking immunity in the Syrian hamster model.

Results

Vaccine virus stability and in vitro safety profile

Both SCV candidates were obtained using a DNA-recombination-based method described previously (Fig. 1a and Supplementary Fig. 1a, from

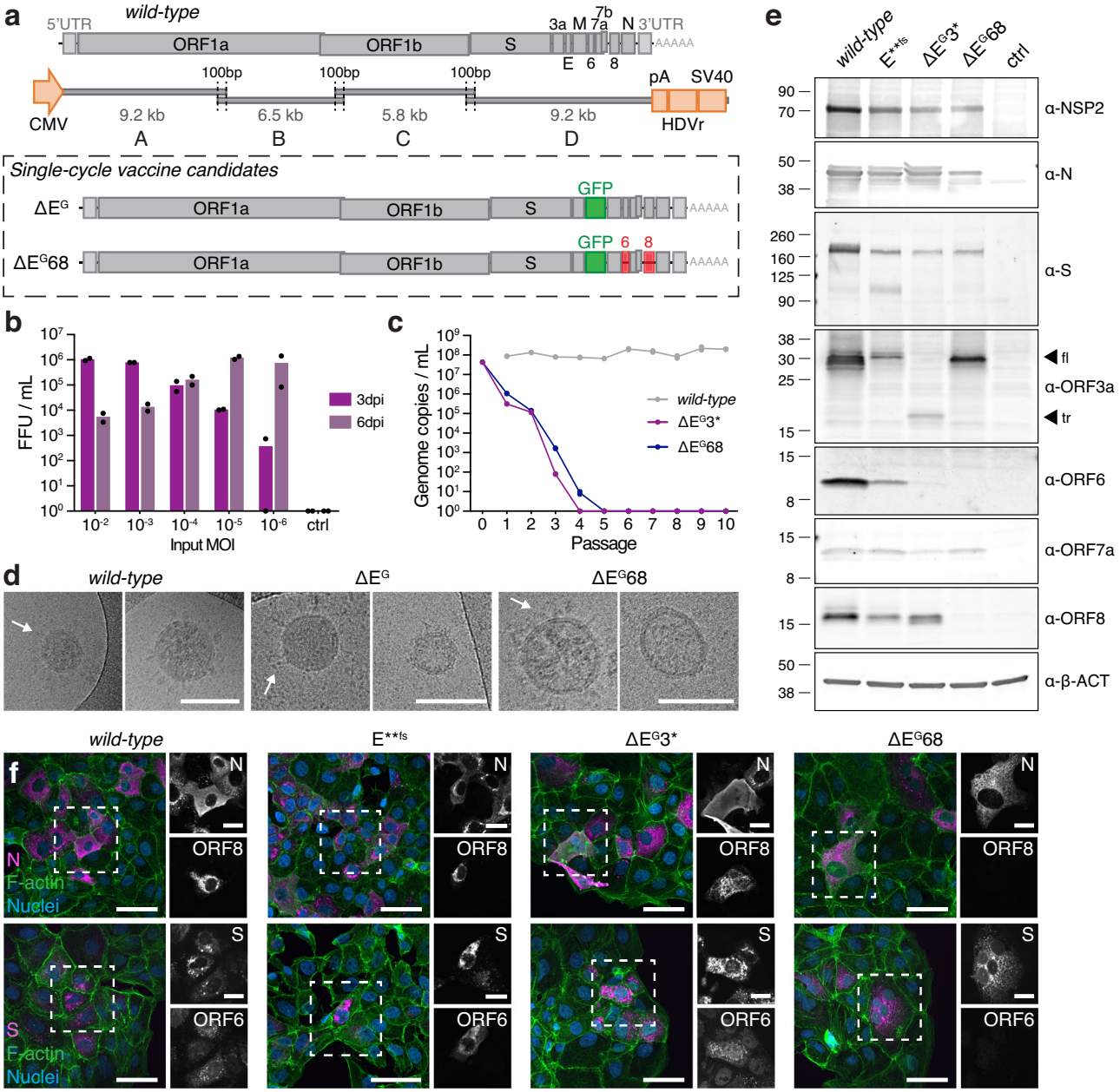

Fig. 1 | Single-cycle vaccine concept and viral characterization. a Schematic illustrating the SARS-COV-2 genomic landscape and the deletions/substitutions in ΔE^G/ΔE^G68, main structural and accessory proteins indicated. Four overlapping fragments covering the whole SARS-CoV-2 genome were amplified by PCR (Fragments A-D, see also Supplementary Fig. 1a). **b** Complementation efficiency of Vero-E2T cells, analyzed by FFU (focus forming units) quantification after infection with ΔE^G3* (ΔE^G with an additional stop codon in ORF3a) at different multiplicities of infection (MOI) or medium-only control (ctrl) three and six days post-infection ($n = 2$ individual cultures), for corresponding genome copies, see Supplementary Fig. 1d. **c** Passaging of 1:10 and 1:100 (after p2) dilutions of cell-free supernatant (Input = Passage 0) of *wild-type* SARS-CoV-2 (Muc-1, B.1), ΔE^G3* and ΔE^G68 on non-complementing Vero E6 cells (initial infection MOI = 1). Data from one representative experiment are shown; analysis was performed in duplicates. **d** Transmission electron microscopy analysis of recombinant *wild-type* SARS-CoV-2 (rCoV2) or vaccine candidates ΔE^G and ΔE^G68 showing the presence of the characteristic spike protein (indicated with arrows). **e** Immunoblot analysis of viral protein production in Vero E6-TMPRSS2 cells infected for 24 h with rCoV2, E**fs, ΔE^G3*, ΔE^G68 or medium only (ctrl), probed with anti-NSP2, anti-N, anti-S, anti-ORF3a (full-length [fl] and truncated [tr] forms indicated with arrows), anti-ORF6, anti-ORF7a, anti-ORF8, and anti-beta-actin (β-ACT) antibodies. **f** Detection of N and S (magenta), F-actin (green), nuclei (blue) and ORF6 or ORF8 in Vero E6-TMPRSS2 cells infected with rCoV2, E**fs, ΔE^G3* or ΔE^G68. Scale bar is 100 nm in (**d**), 50 µm and 20 µm in (**f**) (overview and ROI images, respectively).

design to vaccine virus in ~4 weeks)[26,27]. $\Delta E^G 68$ and ΔE^G were efficiently rescued in E-complementing HEK293T cells (HEK293T-indE) and propagated in a Vero E6-based cell line that stably expresses the E protein (Vero-E2T, additionally expresses ORF6, ORF7, ORF8 and TMPRSS2), verified by qPCR (Supplementary Fig. 1b, c) or propagation of cell-free progeny virus (Fig. 1b and Supplementary Fig. 1d–f). SCV production was monitored by antigen rapid tests[27] and quantified in focus formation assays (FFA).

The precise deletions in vaccine virus candidates $\Delta E^G 68$ and ΔE^G and a stable functional elimination were verified after repeated passage in Vero-E2T cells by high throughput (NGS) and Sanger sequencing (not more than 11 changes outside manipulated regions after 8 passages; no reversion to *wild-type*). Upon repeated passaging, we observed a spontaneous frameshift mutation in ORF3a for candidate ΔE^G, introducing a translational stop codon. This mutation did not change viral properties but consistently led to higher viral load levels in the culture media. Thus, for high multiplicity of infection (MOI) experiments and in vitro safety passaging, $\Delta E^G 3^*$ (ΔE^G with an additional translational stop codon in ORF3a) was applied, while the initial ΔE^G candidate was used in animal studies.

The single-cycle nature of the genetically modified vaccine candidates $\Delta E^G 68$ and ΔE^G was demonstrated by infecting standard Vero E6 cells, a commonly used cellular host: even after a high MOI infection, virus levels in the culture media rapidly declined from passage to passage, corresponding to the dilution steps of the virus passage. This loss was in strong contrast to passages of the *wild-type* virus (Fig. 1c). Any possible emergence of viral revertants at sub-detection levels in Vero E6 cells was excluded by re-passaging supernatant from passages 1 to 10 back on the producer cell line Vero-E2T for 6 days. We demonstrate that 1–5 focus-forming units (FFUs) are sufficient to initiate a rapid viral amplification on Vero-E2T cells (Fig. 1b), indicating that even low-level revertants or newly emerging replicative viral variants would have been detected. None of the passages from passage 4 ($\Delta E^G 68$) or passage 3 ($\Delta E^G 3^*$), led to any rescuable replicative virus with a detection cut-off of 100 genomic copies/mL (Supplementary Fig. 1e, f).

To further verify that SCVs produce authentic viral particles packaging E-defective genomes, virions were analyzed by transmission electron microscopy. The efficient production of spike-carrying spheres with the expected size of 80–100 nm typical for SARS-CoV-2 virions was demonstrated (Fig. 1d). To determine the relative levels of viral S protein produced by the vaccine candidates, surface labeling of cells infected with SCVs or *wild-type* control was performed. Vaccine candidates show a strong S-signal at cell-to-cell interfaces compared to a more clustered staining of cells infected with *wild-type*. This may suggest certain differences in the viral assembly and particle formation process (Supplementary Fig. 1g)[28].

Molecular characterization of vaccine candidates in vitro

Viral protein expression of $\Delta E^G 68$ and $\Delta E^G 3^*$ in infected Vero E6-TMPRSS2 cells (Vero E6 cells stably expressing TMPRSS2, Supplementary Fig. 1b) was determined by immunoblotting (Fig. 1e) and immunocytochemistry (Fig. 1f). As a control, we included the E-defective mutant E^{**fs} (with two back-to-back stop codons [*] and a single G-nucleotide frameshift [fs] insertion after the first 7 amino acids of E) that largely retains RNA sequence and secondary structure. After infection, viral protein levels were found to be similar to the *wild-type* virus (Fig. 1e, f). Also, the expression levels of NSP2 (non-structural protein 2, as reference for virus input), Nucleocapsid protein (N), and S were comparable. For $\Delta E^G 68$, the absence of ORF6 and ORF8 was confirmed, while ORF7 as the interjacent gene remained expressed in all tested variants. Immunoblot data also confirmed the expected ORF3a truncation in $\Delta E^G 3^*$ (Fig. 1e).

In summary, both $\Delta E^G 68$ and ΔE^G vaccine candidates possess close-to-*wild-type* expression levels of all structural components, similar particle shapes, and strict single-cycle properties in standard cells. This molecular characterization led us to verify the immunizing performance of our single-cycle vaccines in vitro and in vivo.

Immuno-modulatory responses in vitro

Immune-downmodulation has been observed for ORF6 and ORF8, and to a lesser extent, for the Envelope protein[20–22,29,30]. To test whether the deletions of E, ORF6, and ORF8 in the SCV lead to a stronger immune response than the *wild-type* virus, we transiently expressed each gene in monocytic THP-1 cells as a model for antigen-presenting cells (APCs). The impact of the newly introduced protein on immunological markers was assessed by cell surface staining of antigen-presenting proteins (HLA-A/B/C, HLA-DR), the co-stimulators CD40, CD44, CD70, CD80, and CD275, and complement cascade protein (CD59) after transfection. We observed downregulation of CD80 and CD275 in response to any of the three proteins (Fig. 2a–c), while no change was observed in the expression of HLA-DR and CD70, thus excluding labeling artifacts (Fig. 2a–c and Supplementary Fig. 2a). The direct effect on HLA-A/B/C was rather modest (Fig. 2a–c and Supplementary Fig. 2b). Taken together, these data support the notion that the expression of ORF6, ORF8, and E correlates with a reduced presentation capacity on APCs.

We then infected alveolar basal epithelial cells (A549-ACE2-TMPRSS2 [A549-AT]) and stained them with the same panel except for HLA-DR. Two different SARS-CoV-2 strains were used: the original Wuhan strain (B.1), which is the basis of our mutants, and the recent Omicron XBB.1.5 strain, which naturally contains a premature stop codon at position 8 of ORF8[31]. A549 cells downregulated HLA-A/B/C and CD275 when infected with the Wuhan strain, but not with $\Delta E^G 68$, whereas Omicron XBB.1.5 and E^{**fs} show only partial downregulation, evoking a role of ORF8 (Fig. 2d, e). Similar effects were observed after infection of HEK293T-ACE2 cells (Supplementary Fig. 2c–e).

Culture supernatant from infected A549-AT or HEK293T-ACE2 cells was then transferred to non-infectable THP-1 cells for 48 h before staining (Supplementary Fig. 2f). For HLA-A/B/C and CD80 we observed the reversed effect of the deletion as seen in overexpression experiments: receptor expression was downregulated by *wild-type* infection, while $\Delta E^G 68$ promoted higher expression (Fig. 2f–i). The intermediate expression levels after infection with E^{**fs} suggest that E and ORF6/ORF8 possess additive, non-overlapping functions. Moreover, the observation that infected as well as non-infectable cells show the same effect suggests that functions of the ORFs themselves rather than the infection event influenced antigen presentation.

Vaccination and challenge infection in the Syrian hamster model

For in vivo testing, hamsters were immunized with $2.4 * 10^4$ FFUs of $\Delta E^G 68$ ($n = 12$) or $3.5 * 10^2$ FFUs of ΔE^G ($n = 8$) in 100 µL per animal (Supplementary Fig. 3a, b). Vaccine candidates or conditioned culture medium-only control (sham) were administered intranasally to 5- / 6-week-old Syrian hamsters, a widely used infection model for safety and efficacy due to their high susceptibility to SARS-CoV-2 and a highly efficient viral spread. A 100% transmission rate for similar doses of full-length SARS-CoV-2 virus in Syrian hamsters has been well described[32,33].

Co-housed naïve contact hamsters were separated for 24 h just before prime or boost immunization or challenge infection (Fig. 3a). Following immunization, all animals continually gained weight as expected for young hamsters, validating in vivo safety (Fig. 3b and Supplementary Fig. 3c). A minor 'dip' in mean body weight observed on days 2–3 in all experimental groups, including contact animals (Fig. 3b), is attributable to procedural stress. Overall, the weight curves indicate that both vaccine candidates were well-tolerated.

The high safety profile of $\Delta E^G 68$ and ΔE^G was further confirmed by rapidly declining levels of vaccine RNA at 3 days post-immunization (dpim; $5 * 10^4$ or $6 * 10^3$ mean genome copies/mL, resp.) compared to $2 * 10^6$ or $4 * 10^4$ RNA copies administered per animal, respectively. At 7 dpim, levels were at or below the quantification threshold of the assay (Supplementary Fig. 3d, e, grey area [≤1000 genome copies/mL]). After boost immunization, a low signal for vaccine RNA was detected on day 3 in two out of 12 animals immunized with $\Delta E^G 68$. On day 7, no vaccine RNA was

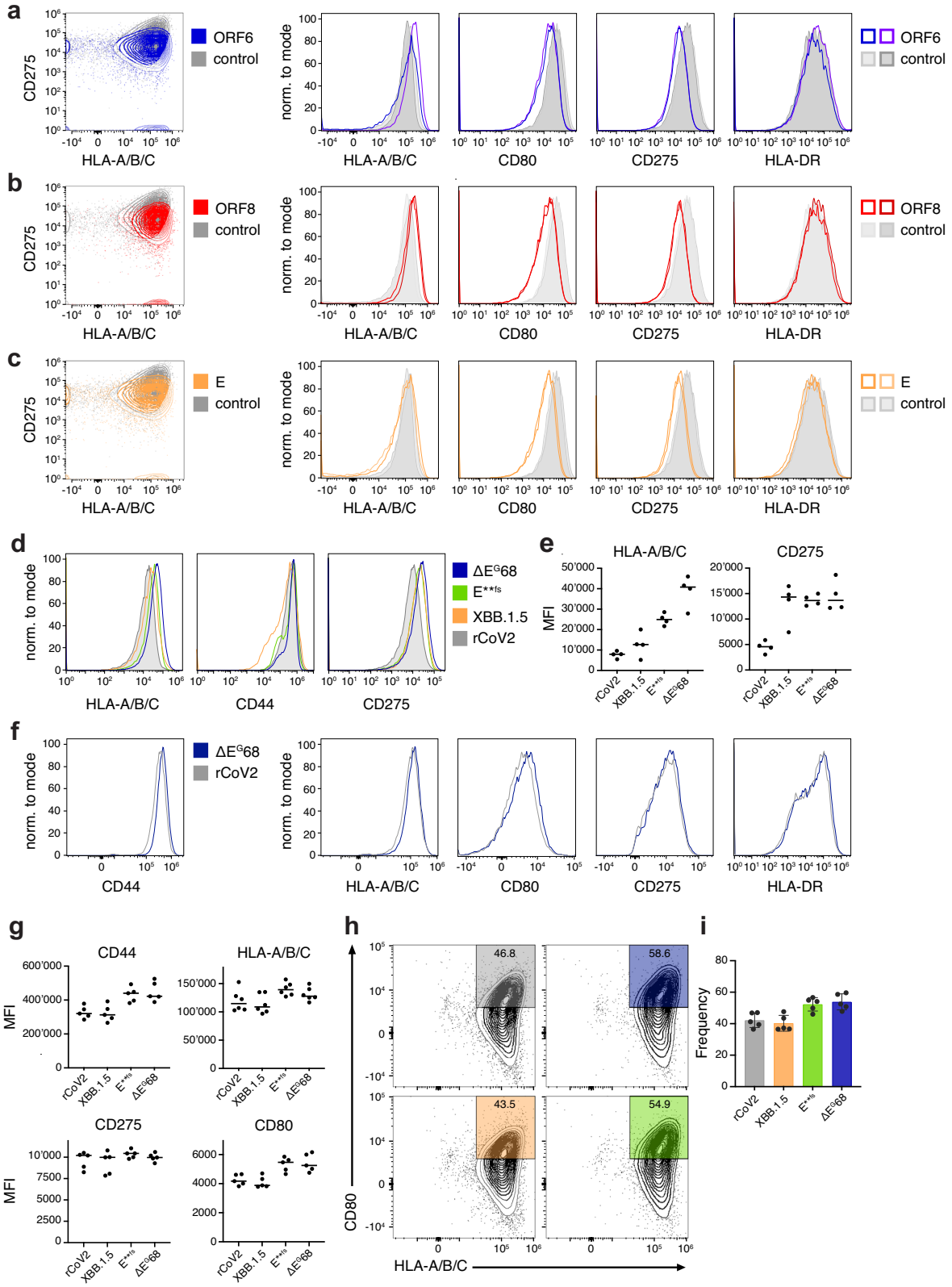

Fig. 2 | Immunomodulation by E, ORF6 and ORF8 proteins. a–c Modulation after transfection: Flow cytometry staining of THP-1 cells for HLA-A/B/C, CD80, CD275, and HLA-DR surface expression 48 h after transfection with expression plasmids for ORF6 (**a**), ORF8 (**b**), or Envelope (**c**) proteins, compared with control transfection. **d–i** Modulation after infection: **d** A549-ACE2-TMPRSS2 cells were infected with recombinant *wild-type* (rCoV2), E**fs, ΔE^{G}68, or XBB.1.5 SARS-CoV-2 virus (MOI = 0.1) for 24 h and stained for HLA-A/B/C, CD44 and CD275. **e** Median fluorescence intensity (MFI) of HLA-A/B/C and CD275. The same infection was conducted on HEK293T-ACE2 and their respective supernatant was then applied on THP-1 for 48 h before surface staining and analysis. **f** Histogram showing the expression of CD44, HLA-A/B/C, CD80, CD275, and HLA-DR on THP-1 after 48 h. **g** Median fluorescence intensity of CD44, HLA-A/B/C, CD80, and CD275 markers on THP-1 after 48 h incubation. **h** Comparison of *wild-type* or ΔE^{G}68 conditions for their expression of CD80 and HLA-A/B/C. The frequency of cells inside the gate in (**h**) is shown in (**i**). Median is shown for (**e**) and (**g**), mean and S.D. for (**i**). The gating strategy is shown in Supplementary Fig. 2g.

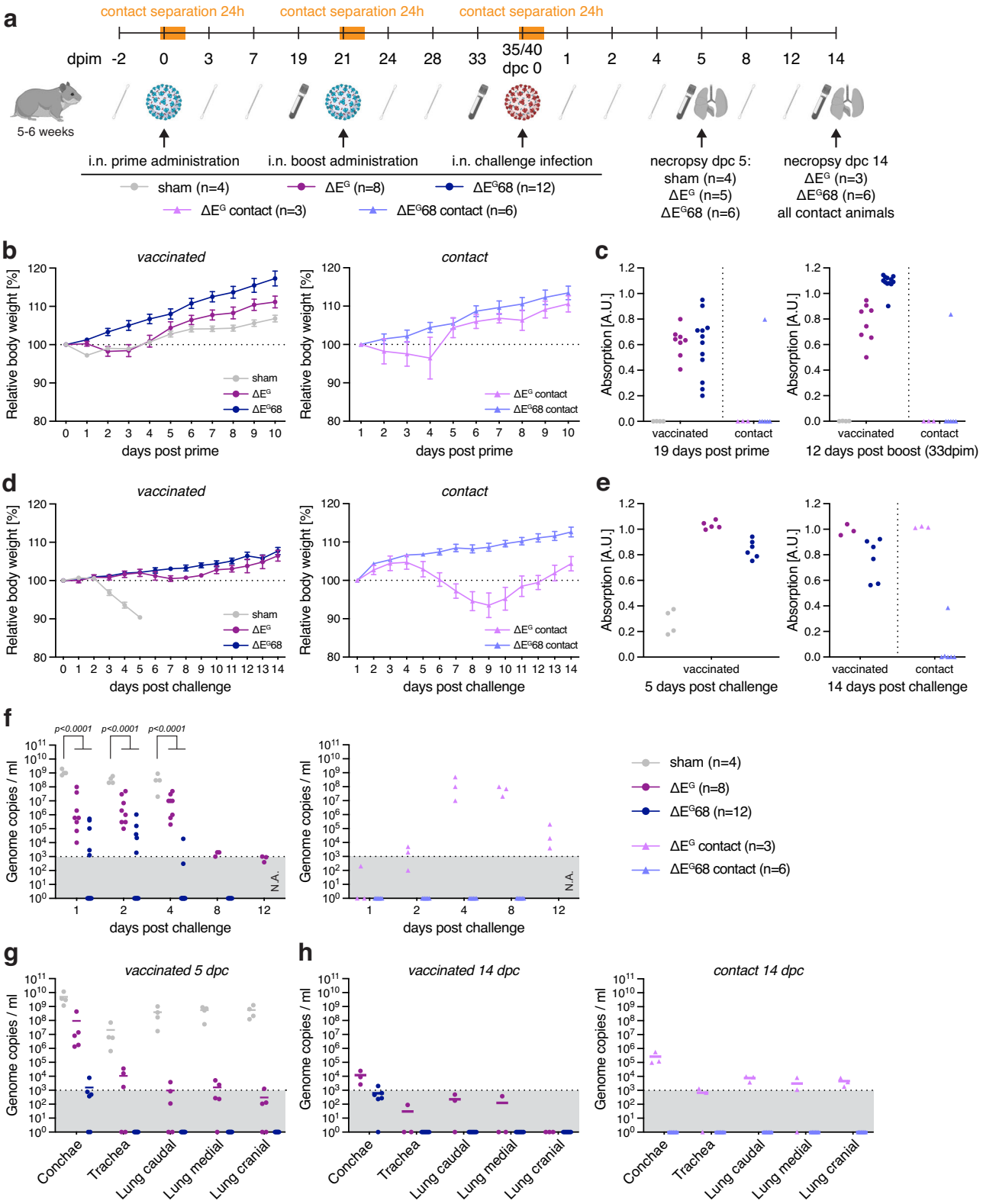

detectable in any of the ΔE^G or ΔE^G68 immunized or contact animals (Supplementary Fig. 3d, e).

On 3 dpim, two ΔE^G68 contacts became positive with a mean of $3 * 10^3$ genome copies/mL (Supplementary Fig. 3d, right). E-gene-specific RT-qPCR[34] verified the deletion of E in the detected RNA and excluded the possibility of a virus reversion (Supplementary Table 2). This was further strengthened by the lack of clinical signs and the absence of any further virus spread (Fig. 3b and Supplementary Fig. 3d, e), indicating a passive transfer of residual ΔE^G68 inoculum.

By 19 dpim, robust SARS-CoV-2 specific humoral immune responses were confirmed in all animals vaccinated with ΔE^G68 or ΔE^G and were even more pronounced after the second immunization (33 dpim) (Fig. 3c). The presence of SARS-CoV-2 specific antibodies on 19 and 33 dpim in one ΔE^G68 contact hamster (Fig. 3c, light blue)

Fig. 3 | Immunization and challenge infection of Syrian hamsters. a Experimental setup and timeline including a prime-boost-immunization with both vaccines or sham (culture medium only) controls and subsequent virus challenge. At indicated time points serum and nasal washing samples were taken. Organ samples were obtained on the days of necropsy. Serum samples were used to detect SARS-CoV-2 RBD (receptor binding domain)-specific antibodies by ELISA or neutralizing antibodies. Genomic RNA loads in nasal washings and organ samples were investigated by SARS-CoV-2 polymerase gene-specific RT-qPCR. **b** Relative body weight after intranasal prime for vaccinated (left) and contact animals (right). **c** Humoral immune response after prime and boost immunization (dpim 19 and 33, resp.), determined by ELISA detecting antibodies against the SARS-CoV-2 RBD of S. **d** Relative body weight after *wild-type* challenge for vaccinated (left) and contact animals (right). **e** Humoral immune response after challenge (5 and 14 dpc), determined by SARS-CoV-2 RBD specific ELISA. **f** Virus genome copy numbers detected in nasal washing samples following challenge infection (note: no data available for ΔE^G68 and ΔE^G68 contact animals at 12 dpc). Viral genome copies in organ samples 5 dpc (**g**) and 14 dpc (**h**). Mean and S.E.M. (**b**, **d**), scatter plots (**g**, **h**) show mean values as line, two-way ANOVA followed by Bonferroni's test (**f**), qPCR assay threshold depicted by grey area. Illustrations in (**a**) were created with BioRender.com.

correlated with the low virus RT-qPCR signal observed at 3 and 7 dpim (Supplementary Fig. 3d).

Following homologous challenge infection with *wild-type* SARS-CoV-2 virus (~ $10^{2.5}$ $TCID_{50}$, Wuhan B.1), no weight loss was observed in the ΔE^G68- and ΔE^G-vaccinated groups, while all sham-vaccinated animals lost body weight until 5 days post-challenge infection (dpc) (Fig. 3d). Sham animals had to be euthanized as per ethical study protocol at 5 dpc. Interestingly, the high levels of a pre-challenge antibody response did not further increase after challenge infection (Fig. 3c, right panel compared to Fig. 3e). This argues for highly protective immunity and antibody induction already during the boost immunization phase, as only very low viral loads (close to the threshold of quantification, grey area) were recovered from nasal washes on days 1, 2, and 4 after challenge infection of the ΔE^G68 vaccinated animals (Fig. 3f). This was in sharp contrast to and significantly different from the situation in sham-vaccinated animals ($p < 0.0001$ for all three time points, Fig. 3f), from which 10^7–10^9 copies/mL were recovered. No viral genomes in nasal washing samples and no weight loss were observed in 6 out of 6 contact animals after challenge infection (Fig. 3d, f, light blue triangles). The full protection of contact animals strongly supports the notion of transmission-blocking immunity achieved by the ΔE^G68 single-cycle vaccine.

Weight loss in ΔE^G contact animals was greatly delayed compared to infected controls starting only at day 3 (Fig. 3d, light purple triangles). The difference in weight loss onset and severity can be explained by reduced challenge virus shedding of ΔE^G immunized animals, which was significantly lower than in sham-immunized controls ($p < 0.0001$ for 1, 2, and 4 dpc, Fig. 3f). This led to low challenge virus infection in the contact animals, and at 4 dpc, the onset of prominent virus replication in the contact hamsters by far exceeded the shedding levels of the vaccinated animals (Fig. 3f, dark purple left panel vs. light purple right panel).

Upon detailed organ examination of ΔE^G68 immunized animals 5 dpc, a low viral load near the quantification limit was restricted to the nasal respiratory tract (Fig. 3g). On day 14 post-challenge, the RNA levels in the conchae of ΔE^G68-vaccinated animals were undetectable or below a quantifiable level. No signal was detected in the trachea or lungs of any of the animals (Fig. 3h).

For ΔE^G, RT-qPCR revealed quantifiable viral loads only in the conchae, calculated to be at least 50-fold lower than in the sham-immunized animals, and nearly complete protection from virus replication was confirmed in lung tissues (Fig. 3g). On day 14 dpc, the RT-qPCR signal in the conchae and the lower respiratory tract was greatly reduced (Fig. 3h). This indicates a high level of protection achieved with the single-cycle vaccines.

Inflammation, tissue integrity, and humoral immunity

Histopathology of the lung revealed full protection from infection-induced pulmonary atelectasis and SARS-CoV-2 characteristic lesions such as necrotizing bronchitis, vasculitis, and necrosis of the alveolar epithelium in ΔE^G68- and ΔE^G-vaccinated groups (Fig. 4a, b). However, minor findings were recorded in all groups (Supplementary Fig. 4a–d and Supplementary Table 3). Using immunohistochemistry, confluent to diffuse SARS-CoV-2 virus antigen was found in the lungs of sham-treated animals and was absent in ΔE^G68- and ΔE^G-vaccinated groups (Fig. 4c, d and Supplementary Table 3). At 14 dpc, ΔE^G contact animals showed minimal atelectasis and SARS-CoV-2 typical lesions; virus antigen was not detectable. In clear contrast, no lesions were identified in the lungs of ΔE^G68 contact animals (Fig. 4a, Supplementary Fig. 4a-d, and Supplementary Table 3).

A quantitative analysis of cytokine levels (IFNγ and IL-10) in homogenates of the conchae and the lungs 5 dpc showed up to tenfold lower levels in ΔE^G68 vaccinated animals compared to sham animals (Fig. 4e, f). At 14 dpc, the comparison of vaccinated animals and their contacts suggests lower interferon secretion for the ΔE^G vaccinated animals in both organs, but the low number of animals does not allow for a precise comparison (Supplementary Fig. 4e). The absence of infection in contact animals of the ΔE^G68 group was corroborated by low cytokine secretion (Supplementary Fig. 4e, f).

Neutralizing antibody responses were quantified against Wuhan (B.1). In 10 out of 12 ΔE^G68 vaccinated hamsters, neutralizing antibodies were detectable after boost immunization (33 dpim, mean 1:229 for 100% neutralization dose) and remained high after challenge for all vaccinated animals (5 dpc, mean 1:220; 14 dpc, mean 1:140) (Supplementary Fig. 4g and Supplementary Table 4). For the one ELISA-positive contact animal, a weak antibody response was detected on 33 dpim (1:40). For animals vaccinated with ΔE^G, neutralizing antibodies were detected after challenge infection (5 dpc, 1:404; 14 dpc, 1:295) (Supplementary Fig. 4g and Supplementary Table 4). Notably, it can't be excluded that neutralization for ΔE^G would score positively before the challenge, as the obtained serum volume was technically limiting to assess lower dilutions. Only one in four sham animals had a low titer (1:20), ruling out that the rise to neutralizing antibodies was based on the virus challenge. For all ΔE^G contact animals, a very low neutralization titer was apparent at 14 dpc (Supplementary Table 4).

Besides peripheral humoral immune responses and to examine the beneficial effects of a nasal application, i.e., local immunity, homogenates of conchae and lung tissues were analyzed for IgA secretion and neutralizing capacity. To rule out any major effects of the challenge infection, both ΔE^G and ΔE^G68 were analyzed at 5 dpc and compared to sham-vaccinated animals. Both groups confirmed mucosal immunity with significantly higher neutralization and IgA levels for ΔE^G and ΔE^G68 compared to sham controls (Fig. 4g, h).

Taken together, both vaccine candidates provide robust protection in the Syrian hamster. In addition, the ΔE^G68 candidate achieved transmission-blocking immunity in all vaccinated animals.

Immune induction in primary human cells

To assess the immunological responses and the effect of the different deletions on antigen presentation, we designed an in vitro immune activation assay using autologous monocyte-derived macrophages as antigen-presenting cells and evaluated peripheral memory T cell reactivation. Peripheral blood mononuclear cells (PBMCs) were obtained from mRNA-vaccinated healthy donors, all having a high neutralization capacity against *wild-type* SARS-CoV-2 (Supplementary Fig. 5a). PBMCs were differentiated into macrophages through plastic adherence over 7 days and exposed to supernatants from A549-ACE2-TMPRSS2 cells, either non-infected (negative control) or infected with ΔE^G68, E^{**fs} (E protein absent; retained RNA sequence/structure) or rCoV2 (recombinant *wild-type*) at an MOI of 0.1 (Fig. 5a). After 24 h, lymphocytes were taken off for FACS analysis, the gating strategy is represented in Supplementary Fig. 5b.

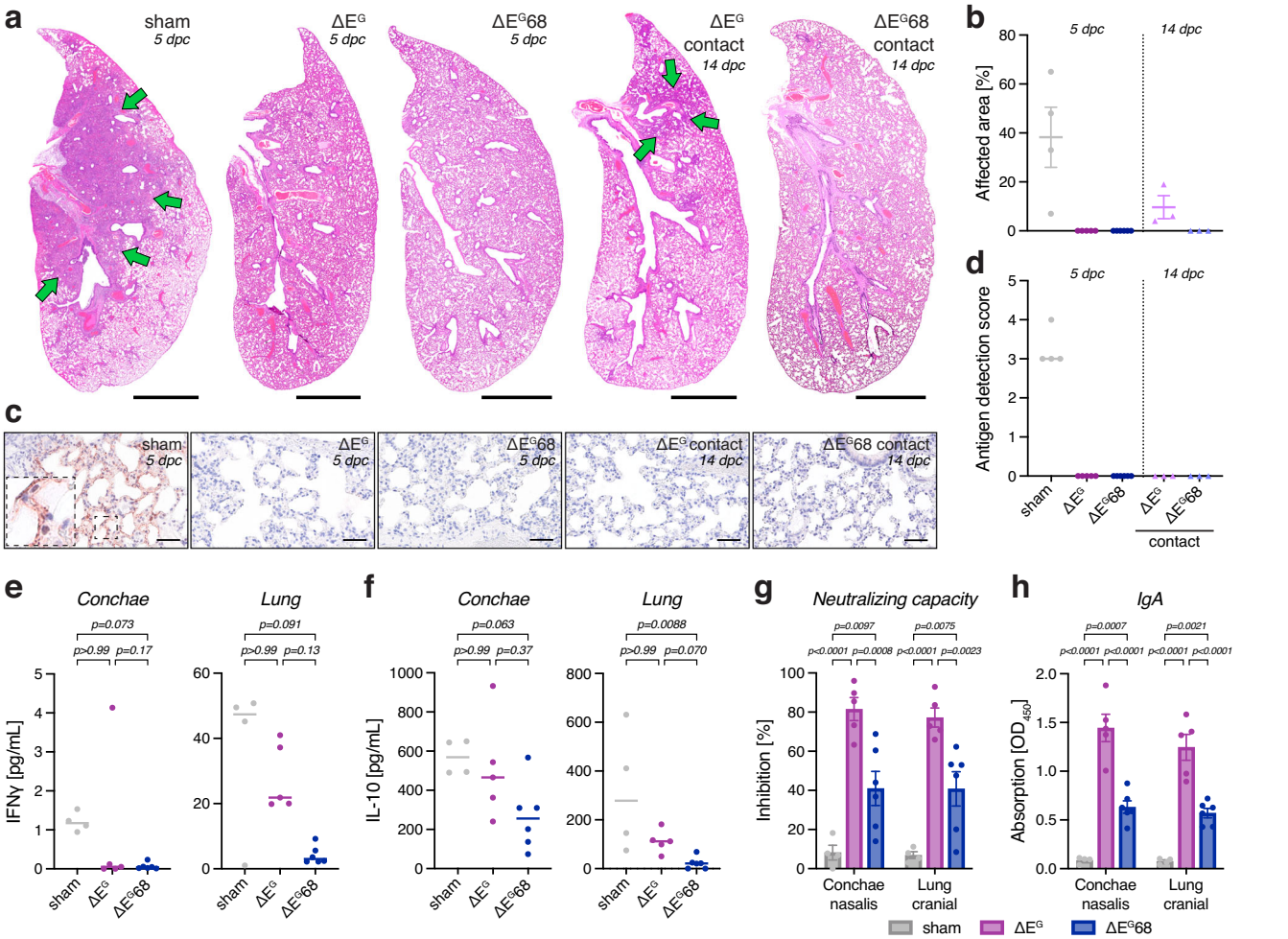

Fig. 4 | Inflammation and tissue integrity. a, **b** Lung histopathology in ΔE^G68, ΔE^G, and sham-vaccinated hamsters or contact animals, 5 or 14 dpc, respectively. Representative whole-slide images of lungs with the affected area indicated by green arrows (**a**) and quantification (**b**) of infection-induced pulmonary atelectasis, affected area per lung lobe. Hematoxylin-Eosin stain, one slide per animal, blind to treatment. **c**, **d** Virus antigen detection in lungs of ΔE^G68, ΔE^G, and sham-vaccinated hamsters or contact animals, 5 or 14 dpc, respectively. Representative immunohistochemistry images showing SARS-CoV-2 nucleocapsid protein detection (**c**) and quantification (**d**) with virus antigen score (semiquantitative, 0 = no antigen, 1 = focal, 2 = multifocal, 3 = coalescing, 4 = diffuse) (Supplementary Table 3). One slide per animal, blind to treatment. Cytokine levels in conchae and lungs of ΔE^G68, ΔE^G, and sham-vaccinated hamsters 5 dpc, ELISA for IFNγ (**e**) and IL-10 (**f**). Neutralizing capacity (**g**) and SARS-CoV-2 specific IgA levels (**h**) in conchae and lungs of ΔE^G68, ΔE^G, and sham-vaccinated hamsters 5 dpc. Number of animals: ΔE^G68 ($n = 6$), ΔE^G ($n = 5$), sham-vaccinated hamsters ($n = 4$), contact animals ($n = 3$ for both groups). Median (**d**, **e**, **f**) or mean and S.E.M. (**b**, **g**, **h**), Kruskal–Wallis (**d**, **e**, **f**) or one-way ANOVA (**b**, **g**, **h**) followed by Dunn's or Bonferroni's multiple comparisons test, respectively. Scale bar is 2.5 mm in (**a**) and 100 µm in (**b**).

Supernatant-exposed macrophages were used to activate autologous T cells of the donor's T cell memory compartment (Fig. 5b–d; $CD3^+$/CD45RA-), crucial for an immune response in pre-exposed individuals. We observed a discernible increase in IFNγ expression in memory T cells exposed to the viruses compared to control (Fig. 5b). Although IFNγ-positive cells represent only a small minority, the difference in the geometric mean fluorescence intensity (gMFI) was statistically significant for E^{**fs}. Furthermore, memory T cells upregulated the expression of activation markers CD69 and CD137 in the two single-cycle conditions (Fig. 5c, d). Moreover, the two single-cycle conditions had a significantly higher proportion of double-positive $CD69^+$/$CD137^+$ memory T cells compared to the control. For the E^{**fs} condition, there was even a significant difference to rCoV2 (Fig. 5e).

The addition of anti-CD107a antibody and Monensin enabled the identification of actively secreting cells. Among CD45RA$^-$, $CD107a^+$ cells, a significantly higher proportion actively secreted IFNγ after ΔE^G68-exposure compared to control and rCoV2 (Fig. 5f). This distinction was also seen when analyzing the strength of the secretion, which was significantly higher for both ΔE^G68 and E^{**fs}, compared to control or rCoV2 (Fig. 5g). The frequency of cells expressing CD69 and/or CD137 was similarly different between the single-cycle condition and negative control (Fig. 5h, i). Of note, even without excluding the unexplained outlier values from one single donor, which were consistently higher across multiple parameters, the observed differences between the viruses used for vaccination remained statistically significant.

Further analysis of memory T cells co-expressing CD137 and CD69 shows higher IFNγ expression levels after ΔE^G68 and E^{**fs} exposure (Fig. 5j), a trend towards higher CD137 expression (Fig. 5k), and a higher CD69 expression for ΔE^G68 compared to control and rCoV2 (Fig. 5l). Notably, the same population had lower CD3 expression than the negative control, indicating TCR-mediated activation and subsequent internalization (Fig. 5m). No changes were observed in HLA-DR or PD-1, indicating that the 24-h time window might be too short after activation to observe differences (Supplementary Fig. 5c). This argues again for a stronger immune activation in the ΔE^G68 group compared to the control, probably mediated by a better antigen presentation.

Discussion

Efficient vaccines must possess key properties to generate a protective immune response. First, they should provide a broad range of epitopes recognized by host antibodies, and second, a significant activation of T

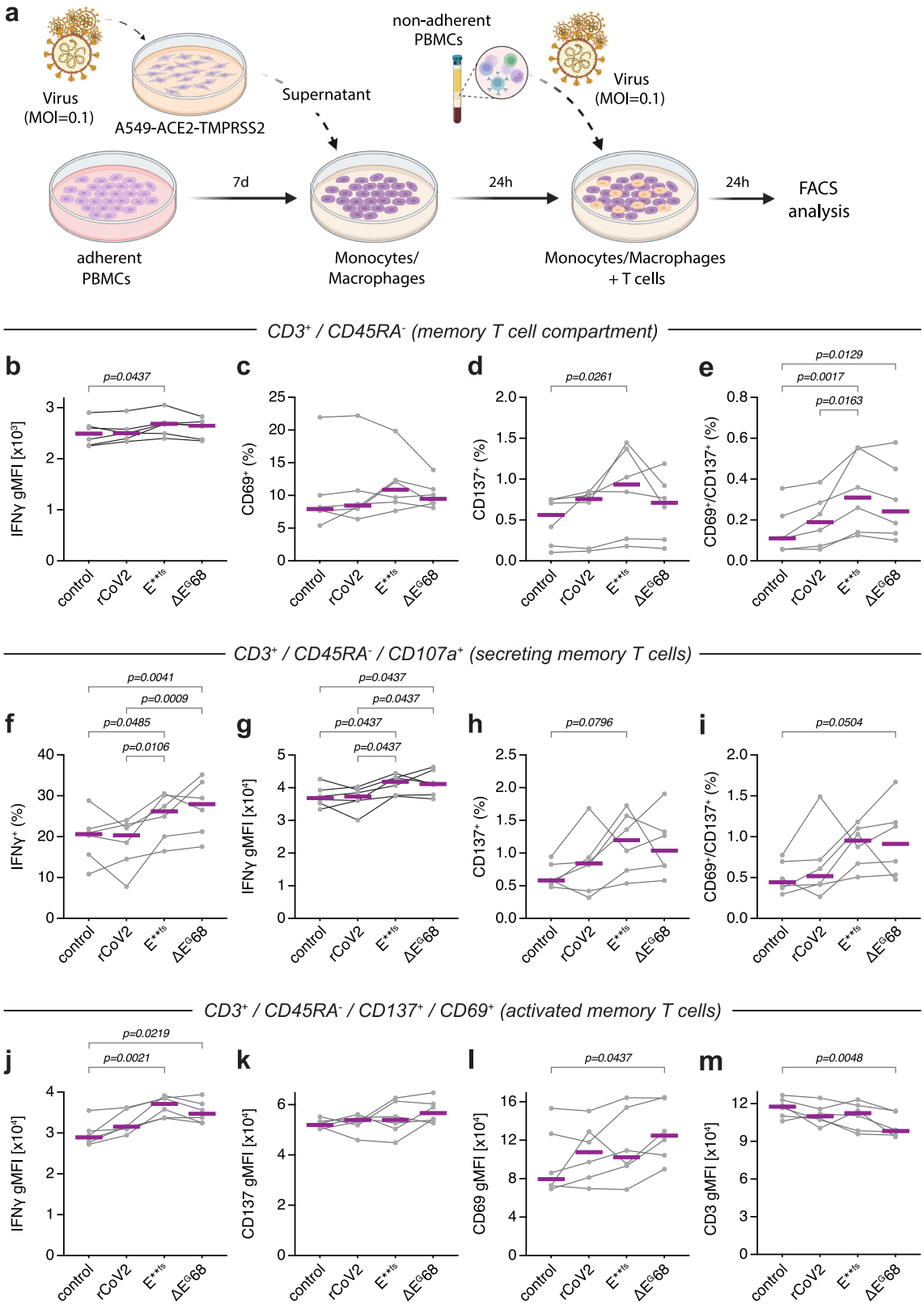

lymphocytes. In addition to strong immunogenicity, it is essential to guarantee maximum safety. The two vaccine candidates reported here combine these properties. Our single-cycle vaccine generates *wild-type*-like viral particles, inducing an accumulation of viral proteins in the host cell, serving as targets for B- and T cells. This implies efficient replication of viral RNA. The deletion of ORF6 and ORF8, two anti-inflammatory proteins antagonizing T cell activation, further supports a robust host response as suggested by our in vitro data and published literature[20–22,28,29].

We demonstrate that both candidates, either lacking E alone or in combination with ORF6 and ORF8, cause higher surface expression of HLA molecules and co-stimulatory factors on infected cells or surrounding APCs, particularly CD80 (B7-1) and CD275 (B7-H1/ICOSLG), both involved in T

Fig. 5 | Autologous PBMC activation after in vitro infection. a General scheme of the experiment, monocytes from vaccinated donors are differentiated into macrophages while a 24-h infection with *wild-type* (rCoV2), ΔE^G68, or E**^{fs} at an MOI of 0.1 is started in A549-ACE2-TMPRSS2 cells. Cellular supernatant is then put in contact with the macrophages for 24 h before matching PBMCs and viruses at an MOI of 0.1 are added. After 24 h, cells are analyzed by flow cytometry ($n = 6$). Comparison of IFNγ geometric mean fluorescence intensity (gMFI) (**b**), frequency of $CD69^+$ (**c**) $CD137^+$ (**d**), and $CD69^+/CD137^+$ (**e**) in the T cell memory compartment ($CD3^+/CD45RA^-$). Comparison of frequencies of $IFN\gamma^+$ (**f**), IFNγ gMFI (**g**), frequency of $CD69^+$ (**h**) or $CD69^+/CD137^+$ (**i**) in actively secreting memory T cells ($CD3^+/CD45RA^-/CD107a^+$). Comparison of IFNγ (**j**), CD137 (**k**), CD69 (**l**), and CD3 gMFIs (**m**) in activated T cells ($CD3^+/CD45RA^-/CD69^+/CD137^+$). The gating strategy is shown in Supplementary Fig. 5b. The median is shown for all graphs, Friedman test with Dunn's multiple comparisons (**b**, **g**, **j**–**m**), or one-way ANOVA with Tukey's multiple comparison tests (**c**–**f**, **h**, **i**) were performed, respectively. The Friedman test is based on sample ranking, and due to the limited number of samples compared here, identical p values may result. Illustrations in (**a**) were created with BioRender.com.

cell stimulation[35,36]. Notably, humans with a defective CD275 gene produce low levels of IgG, IgA, and memory B cells[37]. The single-cycle virus induces stronger activation and cytokine secretion in reactivated Memory T cells of vaccinated individuals ex vivo compared to the *wild-type*. The observed TCR downregulation and the higher IFNγ secretion both suggest more efficient antigen presentation and stronger cytokine support by the single-cycle virus. For some immune markers, E**fs induced a stronger response compared to E^G68, which is most likely due to its higher fitness. As previously described, deletion of ORFs further attenuates the SARS-CoV-2 virus which has benefits considering the individual ORF role in immune modulation and milder clinical manifestation as described recently[23,24]. Thus, ΔE^G68 is preferred over a simple single E-deleted candidate as a potential vaccine candidate. In vivo, these properties could contribute to the development of a lasting and comprehensive immunity. In summary, these elements argue for greater immunogenicity of the SCV compared to its native counterpart.

Furthermore, we achieved transmission-blocking immunity for ΔE^G68 in Syrian hamsters, a fundamental characteristic to prevent viral spread at the population level, not achieved in other vaccine candidates so far[38,39] potentially due to a stronger immune response by IFN-mediated signaling and improved immune stimulation. Especially enhanced local immunity after nasal application, preventing viral shedding[40], was demonstrated by profound IgA and neutralization levels in tissue homogenates of conchae and lung. As the challenge itself only induces a minor response (as seen for the sham control), this is induced by the vaccine virus in both vaccinated groups. Interestingly both immune correlates showed higher values in ΔE^G than in ΔE^G68. Differences in response, i.e., higher values for ΔE^G, could be based on the optimal neutralization efficacy of ΔE^G68, leading to reduced/no boost in the immune response after challenge infection. Consequently, if the challenge virus is quickly neutralized, as seen in ΔE^G68 animals, the "residual challenge infection" induced boost in antibody secretion is weaker compared to the ΔE^G animals, which do not neutralize the virus as efficiently.

The analysis of cytokine secretion additionally highlights the remarkable efficiency of the SCV concept. In the conchae and the lungs, little to no signs of local inflammation were seen at 5 dpc in the ΔE^G68 vaccinated animals, supported by the absence of viral antigens and by the absence of pulmonary lesions observed in histological sections.

Maximum safety of our vaccine approach is ensured by the demonstrated single-cycle concept, in the very sensitive pre-clinical Syrian hamster model. Our concept prevents viral propagation, and unlike an approach using an attenuated virus, which relies on the immune system to combat a weakened virus, could enable the use even in severely immunocompromised people.

In the current post-pandemic situation, almost every individual should have a ground immunity either through vaccination or a wild-type infection. Thus, our vaccine would be considered a booster vaccine. With our recently described CLEVER method[27], we can easily and quickly adapt our SCV vaccines to any arising new variants of concern or interest. This could further improve adapted mRNA vaccines, which currently do not prevent vertical transmission to naïve humans (also not achieved in the hamster system)[9,41,42]. Moreover, the rapid clearance of the non-replicative vaccine virus itself happens in all vaccinated individuals without causing any harm.

Interestingly, we observed the transmission of the higher-dosed ΔE^G68 vaccine to one of six contact animals. RT-qPCR excluded spontaneous genetic reversion, and no further propagation or weight loss occurred, indicating a clear case of passive vaccine virus transfer. This transfer was accompanied by seroconversion, implying that even a minimal dose of the SCV is sufficient to induce a strong serological response. While passive vaccine transfer is highly unlikely in humans, it's essential to carefully consider dosage and application in clinical trials, whether through small-volume sprays or freeze-dried inhalation. It is important to note that the liquid volume used for hamster inoculation was at the upper limit for nasal application in these animals, which typically engage in close nose-to-nose contact.

It should be mentioned here that we had to repeat one SARS-CoV-2 challenge infection, four days following the first infection attempt, due to an erroneous over-dilution with no detection of infectious challenge virus (see Materials and Methods). However, all experimental data confirm that this had no influence on the overall results and that the repeated challenge infection could be classified as fully valid.

Taken together, our proposed single-cycle vaccine concept consolidates the high safety of an intranasally applied vaccine that induces transmission-blocking immunity, which will be key to overcoming ongoing SARS-CoV-2 outbreaks, especially in vulnerable groups.

Methods

The experimental objective was to characterize and evaluate the potential of SCVs as vaccines against SARS-CoV-2 in vitro and in vivo. For the evaluation process, cell cultures (described in detail in Cell lines) and animal models (described in detail in Animals) were used as study subjects. All experiments were controlled laboratory experiments. Animals' conditions were examined daily and verification of vaccine/challenge virus included RT-qPCR-based techniques as well as Histological and Immunohistochemical procedures. The sample sizes and data collection endpoints were chosen based on previous experiments and literature surveys. No data was excluded and all outlier values are displayed. Experiments were performed at least in replicates and measurements were done in technical replicates or triplicates.

Human samples

Human blood samples for peripheral blood mononuclear cell (PBMC) isolation and neutralization assays were collected from SARS-CoV-2 vaccinated or/and infected (within 4 months) donors, aged 29–66 (median 32), who gave their informed consent. All donors were vaccinated with mRNA vaccines (Moderna or Pfizer/BioNTech) and 5 out of 6 had reported infections with SARS-CoV-2.

Animals

Specific pathogen-free male Syrian hamsters (*Mesocricetus auratus*) (Janvier labs, RjHan:AURA) were kept at 20 to 22 °C and a relative humidity of 45 ± 10% on a 12-h light/dark cycle, fed with commercial rodent chow (Ssniff, Soest, Germany), and provided with water ad libitum. The age of the animals at prime immunization is 5 weeks for ΔE^G and 6 weeks for ΔE^G68. Generally, hamsters underwent a daily physical examination and body-weight routine. Hamsters were euthanized in deep anesthesia using

isoflurane by severing the spinal cord in the area of the occiput and blood withdrawal from the cervical veins.

Cell lines

African green monkey kidney cells (Vero E6) were kindly provided by V. Thiel, Bern, Switzerland, or obtained from the Collection of Cell Lines in Veterinary Medicine CCLV-RIE 0929. Adenocarcinomic human alveolar basal epithelial cells expressing ACE2 and TMPRSS2 (A549-AT) were obtained from NIBSC (A549-ACE-2 Clone 8-TMPRSS2; product number 101006). The THP-1 myelomonocytic leukemia cell line was obtained from the American Type Culture Collection. HEK293T cells were kindly provided by D. D. Pinschewer, University of Basel, Switzerland.

All cells were maintained in DMEM high glucose with 10% fetal bovine serum (FBS) + 1% Penicillin/Streptomycin for general propagation or with 2% FBS + 1% Penicillin/Streptomycin for viral infection experiments. During the initial viral rescue, the JAK-I inhibitor Pyridone 6 (CAS 457081-03-7) was added to a final concentration of 2 µM as well as the NFκB inhibitor QNZ (CAS 545380-34-5) at 20 nM. HEK293T-indE received in addition Doxycycline (Merck, D5207) to a final concentration of 2 µg/mL for induction.

Cell line generation

HEK293T-E cells were generated by transfecting HEK293T with 2 µg plasmid DNA containing the SARS-CoV-2 E gene under CMV promoter control in a pcDNA3.1 background containing a Hygromycin resistance gene. After transfection cells were put in DMEM containing 250 µg/mL of Hygromycin. The selection was kept for two weeks and clones were generated by limiting dilution before E expression was tested by RT-qPCR. The clone that showed the highest RNA expression levels was kept for downstream application.

HEK293T-indE (HEK293T-E Tet:E-IRES-ORF6) cells are a derivative of HEK293T-E with a second-generation lentiviral vector generated with the pCW57-E-IRES-ORF6 (Addgene plasmid #80921) as a transfer vector. The vector codes for SARS-COV-2 E and ORF6 under a Tetracycline inducible promoter. After infection, cells were selected in DMEM containing 20 µg/mL of Blasticidin for two weeks. Cells were analyzed by RT-qPCR for E and ORF6 induction following doxycycline treatment (Supplementary Fig. 1c).

HEK293T-ACE2 cells were obtained by infecting the cells with a 2nd generation lentiviral vector with pHR-PGK_hACE2 (Addgene plasmid #161612) as a transfer vector. Cells were sorted for surface expression of ACE2 stained by Mouse anti-human ACE2 (R&D #FAB9332G).

Vero-E2T cells were generated by transfecting Vero E6 cells with 2 µg of an equimolar plasmid mixture containing the SARS-COV-2 E/ORF6/ORF7a/ORF8 genes in individual plasmids all under the CMV promoter in a pcDNA3.1 background containing a Hygromycin resistance gene. After transfection cells were cultivated in DMEM containing 250 µg/mL of Hygromycin. Human TMPRSS2 expression in Vero-E2T and Vero E6 cells (Vero E6-TMPRSS2) was achieved by infecting the cells with a 2nd generation lentiviral vector pLEX307-TMPRSS2-blast (Addgene plasmid #158458) as a transfer vector. After infection cells were selected in DMEM containing 20 µg/mL of Blasticidin for two weeks and analyzed by RT-qPCR for transgene expression (Supplementary Fig. 1b).

Plasmids and lentiviruses

The genes of interest from the Wuhan strain (B.1) were inserted into the pcDNA3.1 backbone under the control of the CMV promoter for expression. The all-in-E plasmid contains the SARS-CoV-2 genes E and ORF6 under the control of an ELF1α promoter or an IRES sequence, respectively, followed by ACE2 and TMPRSS2 under PGK promoter control separated by a P2A cleavage site in a pcDNA3.1 background. The integrity of all plasmids was verified by Sanger sequencing.

The plasmids required for the generation of second-generation lentiviruses were obtained from Addgene. Lentiviruses were generated by transfecting HEK-293T cells with pCMVR8.74 (RRID:Addgene_22036), pMD2.G (RRID:Addgene_12259), and pLEX307-TMPRSS2-blast (RRID:Addgene_158458) plasmids. The culture medium was changed 5 h after transfection, supernatant was collected 24 h later and filtered through a 0.22 µm filter to remove cellular debris.

Viral genome reconstitution procedures

Virus recovery was achieved as described in ref. 27. In brief PCR fragments (fr A-D) spanning the whole SARS-CoV-2 genome were amplified using the high-fidelity proofreading enzyme Q5® High-Fidelity DNA Polymerase (NEB, M0491L) in a 25 µL reaction volume using respective primers (Supplementary Fig. 1a and Supplementary Table 1). Fragment A contains the heterologous CMV promoter upstream of the 5′ UTR and fragment D contains the poly(A) tail, HDV ribozyme, and SV40 termination signal downstream of the 3′ UTR (Fig. 1a).

Cycling conditions were used as recommended by the manufacturer. Fragments were obtained using the following primer combinations: frA: CMV for + frA-frB rev; frB: frB-frA for + frB-frC rev; frC: frC-frB for + frC-frD rev; frD: frD-frC for + SV40 rev. DNA oligonucleotides used are listed in Supplementary Table 1.

12–30 reactions were pooled and purified by PCR column purification using QIAquick PCR purification kit (Qiagen, 28104). DNA concentration was measured by Nanodrop 1000 (Thermo Fisher) or Quantus (Promega, QuantiFluor® ONE dsDNA System, E4871). DNA was further purified by ethanol precipitation and the final concentration was adjusted to 1 µg/µL in nuclease-free water.

Equimolar ratios of frA, frB, frC, or frD (full-length or harboring gene deletions [ΔfrD]) and all-in-E plasmid were transfected into HEK293T-indE using jetPRIME® (Polyplus, cat. 101000001) as recommended by the manufacturer. 4–24 h post-transfection, the medium was changed to DMEM 2% FBS with the addition of JAK-I inhibitor Pyridone 6 (CAS 457081-03-7) to a final concentration of 2 µM as well as the NFκB inhibitor QNZ (CAS 545380-34-5) at 20 nM and 2 µg/mL Doxycycline and Vero-E2T were added for co-incubation. Every 3–4 days, the medium was exchanged. Screen for virus progeny production was done with SARS-CoV-2 antigen rapid test (Roche, 9901-NCOV-01G) or by cytopathic effect (CPE) in E2T and confirmed by RT-qPCR and FFU (focus forming unit) quantification.

Virus propagation for viral stocks

For *wild-type* controls, clinical isolates Muc-1/BavPat1 (a Wuhan-1-type virus isolate, provided by G. Kochs, University of Freiburg, Germany and by Bundeswehr Institute of Microbiology, Munich, Germany [SARS-CoV-2 Germany/BavPat1/2020, GISAID accession EPI_ISL_406862]), Omicron XBB.1.5 (isolated from nasopharyngeal aspirates of human donors, who had given their informed consent), synthetic SARS-CoV-2 (Wuhan-1, GenBank No. MT108784[43]) or rCoV2 (recombinant Wuhan-1-type virus produced by genome reconstitution[27]), were propagated in Vero E6 cells until CPE was observed.

For deletion mutants, viral particles produced by HEK293T-indE were further amplified in Vero-E2T cells, with additional trans-complementation of the all-in-E plasmid. Viral propagation was observed and monitored by CPE and antigen rapid tests[27] and confirmed by RT-qPCR and FFA.

Final viral stocks were harvested, filtered by 0.2 µm filters to remove cells, and frozen in small aliquots. For each viral stock, the viral titer was determined by RT-qPCR and FFA or titration by plaque-forming assay.

Standard plaque-forming assay

Wild-type viral titers were determined by counting plaque-forming units (PFU) after incubation on susceptible cells. Vero E6 cells were seeded at a density of $4 * 10^6$ cells/96-well flat bottom plate in DMEM 2% FBS and incubated overnight at 37 °C and 5% CO_2. Virus was added 1:10 onto the cell monolayer in duplicates or triplicates and serially diluted 1:2 or 1:3. Plates were incubated for 2 days at 34 °C, 5% CO_2 until plaque formation was visible. For virus inactivation, 80 µl of formaldehyde (15% w/v in PBS) (Merck, F8775) was added for 10 min to the cultures. After this period,

fixative and culture medium were aspirated, and crystal violet (0.1% w/v) was added to each well and incubated for 5 min. Subsequently, the fixed and stained plates were gently rinsed several times with tap water and dried before analysis on a CTL ImmunoSpot® analyser.

RNA extraction for viral quantification and sequencing of viral stocks

Viral RNA was extracted using the automated Promega Maxwell RSC system (Promega, AS4500) using either the Maxwell® RSC Viral Total Nucleic Acid Purification Kit (Promega, AS1330) or the Maxwell® RSC miRNA from the Tissue and Plasma or Serum Kit (Promega, AS1680).

Sanger sequencing

The region of interest was amplified using SuperScript™ IV One-Step RT-PCR System (Thermo Fisher, 12594100) with either 'D2 for' or '26847 for' and '29046N rev' (for primers see Supplementary Table 1). The integrity of the PCR product was checked on agarose gel and subsequently sent for Sanger sequencing to evaluate genome regions affected by deletions/mutations (Microsynth, Switzerland).

Next-generation sequencing (NGS)

Viral RNA was converted to cDNA using a cDNA Synthesis kit (biotechrabbit). cDNA was NGS sequenced using EasySeq SARS-CoV-2 WGS Library Prep Kit (NimaGen, SKU: RC-COV096) on an Illumina NextSeq 2000 system with a P1 flow cell (300 cycles). All NGS sequencing and raw data analysis was done by Seq-IT GmbH & Co. KG.

RT-qPCR quantification of viral and intracellular RNA

For the detection of SARS-CoV-2 RNA, a primer and TaqMan probe set for ORF-1b (Supplementary Table 1) was used as described[44]. For the detection of SARS-CoV-2 E and TMPRSS2, an in-house primer/probe set was used (Supplementary Table 1). For the normalization of mRNA expression, GAPDH was used (Supplementary Table 1). For RT-qPCR, Luna® Universal Probe One-Step RT-qPCR Kit (E3006E) was used according to manufacturer´s protocol. In brief, Master Mix was set up: for one reaction 1 µL of each primer, 0.5 µL Probe, 10 µL of Luna Universal Probe One-Step Reaction Mix (2X), 1 µL of Luna WarmStart RT Enzyme Mix (20X) were mixed and brought to 15 µL with nuclease-free water. 15 µL of Master Mix were mixed with 5 µL RNA and amplified on ABI7500 fast cycler (ThermoFisher) using the following cycling conditions: 10 min 55 °C, 1 min 95 °C denaturation, followed by 45 cycles for 10 s at 95 °C and 30 s at 58 °C.

In vitro passaging for in vitro safety experiments

For viral passaging experiments, Vero E6 cells were infected with an MOI of 1 (based on FFU) for 3–4 h with *wild-type* virus or respective deletion candidates. The cells were then washed and fresh 2% DMEM medium was added. Every second day, supernatant (SN) was passaged on freshly seeded Vero E6 (50% confluency). SNs for passage 1 (p1) and p2 were diluted 1:10, for all subsequent passages, SN was diluted 1:100. All collected passages p1 to p10 were subsequently passaged on Vero-E2T. On day 3 and day 6 post-infection SN was sampled for RT-qPCR and images of cell cultures were taken with a Leica DM IL LED inverted microscope. All conditions were treated equally.

Biochemical procedures

For validation and comparison of vaccine candidate viruses, Vero E6-TMPRSS2 cells were infected with virus variants at an MOI of 0.1. 24 h after infection, cells were washed twice with PBS before lysis in cold 140 mM NaCl, 50 mM Tris-HCL, 1% Triton-X100, 0,1% SDS, 0,1% sodium deoxycholate supplemented with protease and phosphatase inhibitors (ThermoFisher, 1861281). Lysates were centrifuged for 10 min, 16,000 × *g* at 4°C, and supernatants analyzed by Immunoblot. Signals were acquired using an image analyzer (Odyssey CLx, Licor).

Flow cytometry analysis

Transfection. Cells were transfected using JetPrime (Polyplus, 101000001) transfection reagent according to the manufacturer's protocol. Five hours after transfection, the culture medium was replaced. In the case of THP-1 cells, only ¼ of the recommended amount of DNA and reagents were used to avoid toxicity.

Infection. For cytometry experiments, all infections were conducted in DMEM supplemented with 2% FBS using a MOI of 0.1 based on FFU data.

Cell isolation and monocyte differentiation. PBMCs were isolated using Ficoll-Paque density gradient centrifugation. For each donor, 25 million PBMCs were initially obtained and cryopreserved. Subsequently, 2 million PBMCs of each donor were seeded per well of a 12-well culture plate in RPMI medium. The plate was then incubated at 37 °C for 1 h, after which non-adherent cells were collected and frozen, while the adherent cells underwent three consecutive rinses with room temperature PBS. Subsequently, the adherent cells were resuspended in RPMI medium containing 10% FBS and maintained in culture for 7 days before the experiment to induce monocyte-to-macrophage differentiation. No cytokine was added, and the media was changed every second day.

Cellular immune activation. In 12-well culture plates, 100,000 A549-ACE2-TMPRSS2 (A549-AT) cells were seeded and cultured in DMEM containing either 10,000 FFU of rCoV2, E**fs, ΔEG68, or no virus (control). Following a 24-h incubation period, the supernatant was harvested, centrifuged at 1000 × *g* to eliminate cellular debris, and subsequently diluted at a 1:3 ratio. This conditioned supernatant was subjected to the monocyte-derived macrophages (at day 7) from each donor. Following a 24-h incubation period, 2 million non-adherent PBMCs from the respective donor, along with 10,000 FFU of the relevant virus or control, were introduced into the wells. This was accompanied by the addition of Monensin at a final concentration of 2 µg/mL and the anti-CD107a antibody, diluted at a 1:200 ratio, to the culture medium. After 20 h of incubation and 4 h before fixation, Brefeldin A at a final concentration of 5 µg/mL was added to the medium.

Staining and fixation. For primary Lymphocytes, after a 24-h incubation and 4 h post Brefeldin A administration, non-adherent PBMCs were collected, washed in PBS, stained with Zombie UV® Fixable Dead Cell Stain (Biolegend) and subjected to a 20-min incubation in a blocking buffer comprising 50% FBS, Brefeldin A, Monensin, and FcR Blocking Reagent (diluted at 1:200). The cells were subsequently incubated for 30 min to label cell surface proteins in a staining buffer containing an antibody mix. Following this, the cells were fixed and permeabilized using the eBioscience™ Transcription Factor Staining Buffer Set, following the manufacturer's recommendations for intracellular target analysis. Finally, intracellular staining was performed using an anti-IFNγ antibody for 30 min at room temperature. For transfection, cells were washed in PBS and stained with Zombie UV® Fixable Dead Cell Stain (Biolegend), rinsed once with PBS, and blocked in blocking buffer (PBS with 50% FBS), FcR Blocking Reagent 1:150 (Miltenyi Biotec) for 30 min at room temperature, followed by incubation with antibodies against cell-surface molecules in staining buffer (PBS with 15% FBS, FcR Blocking Reagent 1:1000) for 30 min at room temperature. Data were acquired on an Aurora (Cytek, Amsterdam, Netherlands) equipped with 5 lasers (355, 405, 488, 561, and 640 nm) and 60 channels (full spectrum cytometry), unmixed with SpectroFlo®, and analyzed with FlowJo 10.9.0 (TreeStar). The gating strategy is shown in Supplementary Information.

Immunocytochemistry

For detection of infectious vaccine viral particles (focus forming assay [FFA]), protein expression analysis, and surface labeling, Vero E6-TMPRSS2 cells grown on coverslips in 24-well plates were infected with

virus variants in 500 µL DMEM medium supplemented with 2% FBS and 1% Penicillin/Streptomycin and incubated overnight. Cells were fixed with 4% PFA in PBS for 10 min at room temperature, washed, and subsequently stained. For FFU determination and protein expression analysis, cells were blocked with 10% Normal Donkey Serum (Jackson ImmunoResearch, 017-000-121) and 0.1% Triton X-100 at room temperature for 60 min followed by incubation with primary antibodies for 60 min at room temperature or overnight at 4 °C in 1% Normal Donkey Serum, 1% BSA and 0.3% Triton X-100 in PBS. Cells were washed three times for 10 min with 0.1% BSA/PBS and incubated with fluorophore-coupled secondary antibodies for 60 min at room temperature in 1% Normal Donkey Serum, 1% BSA and 0.3% Triton X-100 in PBS. Cells were washed once with 0.1% BSA/PBS and washed three times with PBS before mounting on microscope slides using Fluoromount-G (SouthernBiotech, 0100-01). For surface labeling, cells were blocked with 5% milk powder in PBS at room temperature for 1 h and incubated with primary antibodies in 1% BSA/PBS overnight at 4 °C. After 3 washes with PBS, fluorophore-coupled secondary antibodies in 1% BSA/PBS were applied for 60 min at room temperature and washed three times with PBS before mounting on microscope slides. Phalloidin-iFluor488 or -iFluor555 was co-applied with secondary antibodies to label F-actin (Abcam, ab176753 and ab176756 resp.). Hoechst 33342 dye (Merck, B2261) was co-applied during washing at a final concentration of 0.5 µg/mL for nuclear staining.

Images for FFU quantification were acquired on a bright-field microscope (Nikon Ti2 equipped with a Photometrics 95B camera, Nikon NIS AR software), using a 20x Plan-Apochromat objective (numerical aperture 0.75) and were then processed in Fiji and Omero. For quantification of infected foci, images were analyzed with QuPath[45]. Images for protein expression and surface labeling were acquired on an inverted spinning-disk confocal microscope (Nikon Ti2 equipped with a Photometrics Kinetix 25 mm back-illuminated sCMOS, Nikon NIS AR software), using 40x and 100x Plan-Apochromat objectives (numerical aperture 0.95 and 1.45, respectively) and were then processed in Fiji and Omero.

Electron microscopy

Viral particles were fixed in 1% glutaraldehyde (Thermo Scientific, 233281000). A 4 µL aliquot of sample was adsorbed onto holey carbon-coated grid (Lacey, Tedpella, USA), blotted with Whatman 1 filter paper and vitrified into liquid ethane at −180 °C using a Leica GP2 plunger (Leica microsystems, Austria). Frozen grids were transferred onto a Talos 200C Electron microscope (FEI, USA) using a Gatan 626 cryo-holder (GATAN, USA). Electron micrographs were recorded at an accelerating voltage of 200 kV using a low-dose system (40 e-/Å2) and keeping the sample at −175 °C. Defocus values were −2 to 3 µm. Micrographs were recorded on 4K × 4K Ceta CMOS camera.

Animal immunization and analysis

ΔE^G immunization. Eight hamsters were intranasally inoculated with 50 µL of ΔE^G virus stock per nostril ($3.5 * 10^2$ FFU, Supplementary Fig. 3a, b) at day 0 and boosted with the same dose at day 21. Four hamsters were inoculated with 100 µL of supernatant from uninfected cells and therefore served as sham vaccinated controls. The three direct contact animals were co-housed with ΔE^G immunized animals but were separated for 24 h just prior to immunizations and challenge, respectively. Nasal wash samples were taken on days −2, 3, 7, 24, 28, 36, 37, 39, 43, and 47 post immunization (dpim), by applying 200 µL of PBS into each nostril and collecting the reflux under short isoflurane inhalation anesthesia. Serum samples were taken by puncturing the *V. saphena* at 19 and 33 dpim for serological evaluation. At 35 dpim eight ΔE^G immunized animals and four sham vaccinated control animals (intranasally inoculated with filtered medium of non-infected cells) were challenged by intranasal inoculation using $10^{2.5}$ $TCID_{50}$/animal of SARS-CoV-2 virus (Wuhan-1, GenBank No. MT108784[43]) in a 70 µL volume (calculated from back-titration). Five days post challenge (dpc), five ΔE^G immunized hamsters and the sham vaccinated control hamsters were sacrificed following the ethical protocol approval, and sera as well as organ samples from the upper and lower respiratory tract were collected during necropsy. At 14 dpc, three ΔE^G immunized hamsters and three contact animals were euthanized and serum samples as well as organ samples from upper and lower respiratory tracts were collected during necropsy.

ΔE^G68 immunization. Twelve hamsters were intranasal inoculated with 100 µL of ΔE^G68 virus stock ($2.4 * 10^4$ FFU, Supplementary Fig. 3a, b) at day 0 and boosted with the same dose at day 21. Six direct contact animals were co-housed with ΔE^G68 immunized animals but were separated for 24 h before immunizations and challenge infection, respectively. Nasal washing samples were taken at dpim −2, 3, 7, 24, 28, 36, 37, 38, 41 (dpc1), 42 (dpc2), 44 (dpc4) and 48 (dpc8) by applying 200 µL of PBS in each nostril and collecting the reflux under short isoflurane inhalation anesthesia. Serum samples were taken by puncturing the *V. saphena* at 19 and 33 dpim for serological evaluation. At 35 dpim the ΔE^G68 immunized animals were inoculated using a miscalculated low dosage of SARS-CoV-2 virus (Wuhan-1, GenBank No. MT108784[43]) with less than 1 $TCID_{50}$/animal. The viral genome copies in this highly over-diluted inoculum were determined by RT-qPCR (RNA-dependent RNA polymerase (IP4) as the target[46]) with a Ct-value of 35.64, representing 1089 genome copies / mL. With this sample, we were unable to initiate a productive infection even when 70 µL of pure inoculum was applied to Vero E6 cells (0.32 cm^2, $n = 7$). In addition, all nasal wash samples taken from the animals on the first three days after inoculation were negative by RT-qPCR (Supplementary Table 2). Therefore, the challenge infection was repeated with the same animals at 41 dpim applying 70 µL with $10^{2.3}$ $TCID_{50}$/animal (Wuhan-1, GenBank No. MT108784[43]), calculated from a back-titration. Five days post challenge infection, six ΔE^G68 immunized hamsters were euthanized and serum samples as well as organ samples from the upper and lower respiratory tract were collected during necropsy. 14 dpc six ΔE^G immunized hamsters and their respective six matching contact animals were euthanized and serum samples as well as organ samples from the upper and lower respiratory tract were collected during necropsy.

RNA analysis of hamster samples. RNA from nasal washings and organ samples was extracted using the NucleoMag® VET Kit (Macherey-Nagel, Düren, Germany) in combination with a Biosprint 96 platform (Qiagen, Hilden, Germany). Viral RNA genomes were detected and quantified by real-time RT-qPCR on a BioRad real-time CFX96 detection system (BioRad, Hercules, USA). The target sequence for amplification was viral RNA-dependent RNA polymerase (IP4)[34,46]. Genome copies per mL sample were calculated based on a quantified standard RNA, where absolute quantification was done by the QX200 Droplet Digital PCR System in combination with the 1-Step RT-ddPCR Advanced Kit for Probes (BioRad, Hercules, USA). The detection limit was calculated to be 1000 copies per reaction.

RBD-specific SARS-CoV-2 antibodies in serum. Serum samples were analyzed using an indirect multispecies ELISA against SARS-CoV-2 RBD[47]. Briefly, RBD-coated plates or those treated with coating buffer-only were blocked with 5% skim milk in phosphate-buffered saline, pH 7.5. Serum samples were incubated on the coated and uncoated wells for 1 h at room temperature. Using a multi-species conjugate (SBVMILK; obtained from ID Screen® Schmallenberg virus Milk Indirect ELISA; IDvet) diluted 1/80 for 1 h at room temperature detection was performed after the addition of tetramethylbenzidine (TMB) substrate (IDEXX) at a wavelength of 450 nm. After each step, the plates were washed three times with Tris-buffered saline with Tween 20. For readout, absorbances were calculated by subtracting the optical density (OD) measured on the uncoated wells from the values obtained from the protein-coated wells for each respective sample. Reproducibility was confirmed and normalization was achieved by reference to negative and positive sera samples.

Cytokine measurement. IFN and IL-10 were measured in homogenized hamster organs by ELISA. Organ samples of about 0,1 cm^3 size from hamsters were homogenized in a 1 mL mixture composed of equal volumes of Hank's balanced salts MEM and Earle's balanced salts MEM (containing 2 mM L-glutamine, 850 mg/L $NaHCO_3$, 120 mg/L sodium pyruvate, and 1% Penicillin/Streptomycin) at 300 Hz for 2 min using a Tissuelyser II (Qiagen) and were then centrifuged to clarify the supernatant. 50 µL of this homogenate was then used as a sample according to the manufacturer's instruction with the Hamster IFNγ (Assaygenie #HMFI0010) and Hamster IL-10 ELISA Kit (Assaygenie #HMFI0003) for IFNγ and IL-10 respectively.

SARS-CoV-2–specific IgA from organ homogenates. SARS-CoV-2 specific IgA was detected in the supernatant of homogenates from conchae and lung tissue by ELISA. 96-well, flat bottom ELISA plates (Nunc™ MaxiSorp™) were coated with 100 µL of 1,5 µg/mL recombinant SARS-CoV-2 spike protein (S1+S2 ECD, His tag; Sino Biological) in PBS overnight at 4 °C. The following day, plates were washed three times with PBS supplemented with 0,05% Tween 20 (PBS-T) and incubated with 5% skim milk in PBS (blocking buffer) for one hour at room temperature to block unspecific binding. Organ homogenates were centrifuged at 4000 × *g* for 5 min. Supernatants were diluted at 1:30 in blocking buffer before adding 50 µL of the diluted samples to the plates. Samples were incubated in the plates for two hours at room temperature. The plates were washed three times before adding 50 µL of 1:50 diluted biotinylated anti-hamster IgA detection antibody (Brookwood Biomedical). Following 2 h incubation, plates were washed three times and 50 µL High-Sensitivity NeutrAvidin HRP conjugate was added for 30 min at room temperature. The plates were washed three times and 50 µL 1-Step Ultra TMB ELISA Substrate Solution (ThermoFisher) was added. After five minutes, the reaction was stopped by adding equal volume of 2 M sulfuric acid. The plates were read for absorbance at 450 nm and 570 nm on a Tecan Infinite M200 Pro Microplate reader. Extinction at 570 nm was subtracted as background.

Surrogate virus neutralization test (sVNT). To evaluate specifically the presence of virus-neutralizing antibodies in the supernatant of lung and conchae nasalis homogenates the cPass SARS-CoV-2 Neutralization Antibody Detection Kit (GeneScript Ref: L00847) was used following the kit instructions. In short, homogenized organ samples and controls were diluted 1:10 in Sample Dilution Buffer and mixed 1:1 with 1:1000 diluted RBD coupled horse-reddish peroxidase and incubated at 37 °C for 30 min. 100 µl of the mixture was added to a respective well of the ACE2-coated assay plate and incubated for 15 min at 37 °C. After that the plate was washed and 100 µl TMB Solution was added to the well and incubated for another 15 min in darkness. Finally, 50 µl Stop solution was added and optical density (OD) was measured at 450 nm wavelength. Percentual signal inhibition was calculated by setting the OD450 value in relation to the negative control.

Neutralization assay. To evaluate specifically the presence of virus-neutralizing antibodies in serum samples a live virus neutralization test was performed. Sera were pre-diluted (starting dilution from 1/16 to 1/512) with Dulbecco's modified Eagle's medium (DMEM) in a 96-well deep well master plate. 100 µL of this pre-dilution was transferred into a 96-well plate. A log2 dilution was conducted by passaging 50 µL of the serum dilution in 50 µL DMEM, leaving 50 µL of sera dilution in each well. Subsequently, 50 µL of SARS-CoV-2 (BavPat1) virus dilution (100 $TCID_{50}$/well) was added to each well and incubated for 1 h at 37 °C. Lastly, 100 µL of trypsinized Vero E6 cells (cells of one confluent T-175 flask per 100 mL) in DMEM with 1% Penicillin/Streptomycin supplementation were added to each well. After 72 h incubation at 37 °C, the cells were evaluated by light microscopy for a specific CPE. A serum dilution was counted as neutralizing in the case no specific CPE was visible and is given as neutralizing dose 100 (ND100). The virus titer was confirmed by virus titration; positive and negative serum samples were included. Tests were performed in 3 technical replicates and average values were used to calculate the 100% neutralizing dose with the Kerber formula: (-log2) = a/b + c ((a) cell culture wells without virus replication, (b) number of cell culture wells per sera dilution, (c) -log2 of pre-dilution of the sera sample).

Pathology. For histopathology, the left lung lobe was processed as described[48]. The left lung lobe was carefully removed, immersion-fixed in 10% neutral-buffered formalin, paraffin-embedded, and 2- to 3-µm sections were stained with hematoxylin and eosin (HE). Consecutive sections were processed for immunohistochemistry (IHC) used according to standardized procedures of avidin-biotin-peroxidase complex (ABC)-method[49]. Briefly, endogenous peroxidase was quenched on dewaxed lung slides with 3% hydrogen peroxide in distilled water for 10 min at room temperature. Antigen heat retrieval was performed in 10 mM citrate buffer (pH 6) for 20 min in a pressure cooker. Nonspecific antibody binding was blocked for 30 min at room temperature with goat normal serum, diluted in PBS (1:2). A primary anti-SARS-CoV nucleocapsid protein antibody was applied overnight at 4 °C (1:3000), the secondary biotinylated goat anti-mouse antibody was applied for 30 min at room temperature (Vector Laboratories, Burlingame, CA, USA, 1:200). Color was developed by incubation with ABC solution (Vectastain Elite ABC Kit; Vector Laboratories), followed by exposure to 3-amino-9-ethylcarbazole substrate (AEC, Dako, Carpinteria, CA, USA). The sections were counterstained with Mayer's hematoxylin. As a negative control, consecutive sections were labeled with an irrelevant antibody (M protein of Influenza A virus, ATCC clone HB-64). An archived control slide from a SARS-CoV-2-infected Syrian hamster was included in each run. All slides were scanned using a Hamamatsu S60 scanner and evaluated using the NDPview.2 plus software (Version 2.8.24, Hamamatsu Photonics, K.K. Japan) by a trained (TB) and reviewed by a board-certified pathologist (AB), blind to treatment. The lung was evaluated using a 500 × 500 µm grid, and the extent of pneumonia-associated consolidation was recorded as the percentage of affected lung fields. We examined for the presence of SARS-CoV-2-characteristic lesions as given in Supplementary Table 3. Following IHC the distribution of virus antigen was graded on an ordinal scale with scores 0 = no antigen, 1 = focal, affected cells/tissue <5% or up to 3 foci per tissue; 2 = multifocal, 6%–40% affected; 3 = coalescing, 41%–80% affected; 4 = diffuse, >80% affected. The target cell was identified based on morphology.

Antibodies

The following antibodies were used in this study: mouse monoclonal anti-β-actin (Cell Signaling Technology; 3700; RRID: AB_2242334; LOT# 20), rabbit polyclonal anti-SARS-CoV-2 nsp2 (GeneTex; GTX135717; RRID: AB_2909866; LOT# B318853), rabbit polyclonal anti-SARS-CoV Nucleocapsid protein (Rockland; 200-401-A50; RRID:AB_828403), mouse monoclonal anti-SARS-CoV-2 Nucleocapsid protein (4F3C4, gift from S. Reiche[50]), sheep polyclonal anti-SARS-CoV-2 ORF3a[51], rat monoclonal anti-SARS-CoV-2 ORF6 (8B10, gift from Y. Miyamoto[52]), rabbit polyclonal anti-SARS-CoV-2 ORF8 (Novus Biologicals; NBP3-07972; LOT# 25966-2102), mouse monoclonal anti-SARS-CoV-2 Spike protein (4B5C1, gift from S. Reiche).

Fluorophore-conjugated secondary antibodies were from Jackson ImmunoResearch (Cy3 donkey anti-rat #712-165-153, Cy3 donkey anti-mouse #715-165-151, Cy5 donkey anti-rabbit #711-175-152, Cy5 donkey anti-mouse #715-175-511), Li-Cor (IRDye 680RD donkey anti-mouse #926-68072, IRDye 680RD goat anti-rabbit #926-68071, IRDye 680RD goat anti-rat #926-68076) and Invitrogen (Alexa Fluor 647 donkey anti-mouse #A31571, Alexa Fluor 680 donkey anti-sheep #A21102).

Flow cytometry antibodies (all anti-human) were from Miltenyi REAfinity™ (VioBlue™ anti-CD44 #130-113-344, VioGreen™ anti-HLA-ABC #130-120-436, PerCP-Vio-700 anti-CD59 #130-128-812, PE-Vio®770 anti-CD275 (B7-H2) #130-116-805, APC anti-CD70 #130-130-100,

VioBright V600 anti-IFNγ #130-131-167, Per-CP anti-HLA-DR #130-113-96, PE-Vio770 anti-CD107a #130-111-622, APC anti-CD137 #130-110-764), Biolegend (Brilliant Violet 711 anti-CD80 #305236, Alexa Fluor® 700 anti-HLA-DR #307626, Brilliant Violet 421 anti-CD279 #329920, Brilliant Violet 510 anti-CD3 #300448, Brilliant Violet 650 anti-CD4 #300536, Brilliant Violet 785 anti-CD69 #310931, Alexa Fluor® 700 anti-CD8a #301028, APC/Cyanine7 anti-CD19 #302218) and R&D (mouse monoclonal anti-hACE2 #FAB9332G).

Neutralization assay human samples

Vero E6 cells were seeded in 96-well flat bottom plates, 3.5×10^6 cells / plate in a final volume of 100 µL DMEM complemented with 2% FBS, 1% Penicillin/Streptomycin. Cells were incubated at 37 °C, 5% CO_2 overnight to reach confluency. Patient sera were serially diluted 1:2 in a 96-well round bottom plate, starting with a 1:20 dilution. Virus was added to the diluted sera at a final MOI of 0.002 per well and incubated for 1 h at 34 °C, 5% CO_2. Pre-incubated sera/virus was added to the cells and incubated for 2 days at 34 °C, 5% CO_2. For virus inactivation, 20 µL of formaldehyde (18% w/v in PBS) (Cat# F8775, Sigma-Aldrich) was added for 30 min to the cultures. Fixative and culture medium were aspirated, and crystal violet (0.5% w/v) was added to each well for 5 min. Fixed and stained plates were gently rinsed several times under tap water and dried before analysis on a CTL ImmunoSpot® analyzer.

Statistics

Data were analyzed using GraphPad Prism 9 and 10 software. No statistical methods were used to pre-determine sample sizes. Acquisition and analysis of lung pathology were done by an investigator blinded to the condition. Appropriate statistical tests were chosen based on sample size and are indicated in individual experiments.

Study approval

All experiments involving human donors were approved by Ethikkommission Nordwest- und Zentralschweiz (#2022-00303). All procedures involving animals were in accordance with relevant guidelines and regulations, evaluated by the responsible ethics committee of the State Office of Agriculture, Food Safety, and Fishery in Mecklenburg–Western Pomerania (LALLF M-V) and gained governmental approval under the registration numbers LVL MV TSD/ 7221.3-1-041/20 and 7221.3-1-001/22. All work including infectious SARS-CoV-2 viruses and their recombinant variants was conducted in a biosafety level 3 facility at the Department of Biomedicine within the University of Basel (approved by the Swiss Federal Office of Public Health [BAG] #A202850/3).

Materials & correspondence

This study has generated plasmids, which will be deposited to Addgene. Generated cell lines will be made available upon request. Recombinant viruses will be available through EVA-GLOBAL. Further information and requests for resources and reagents should be directed to and will be fulfilled by the lead contact, Thomas Klimkait (thomas.klimkait@unibas.ch) or by Fabian Otte (fabian.otte@unibas.ch).

Data availability

All sequencing data is deposited at NCBI with the following accession numbers: BankIt2706771, OR061321-OR061337, PRJNA975579.

Received: 5 March 2024; Accepted: 10 October 2024;
Published online: 30 October 2024

References

1. Beesley, L. J. et al. SARS-CoV-2 variant transition dynamics are associated with vaccination rates, number of co-circulating variants, and convalescent immunity. *eBioMedicine* **91**, 104534 (2023).
2. Baden, L. R. et al. Efficacy and safety of the mRNA-1273 SARS-CoV-2 vaccine. *N. Engl. J. Med.* **384**, 403–416 (2021).
3. Polack, F. P. et al. Safety and efficacy of the BNT162b2 mRNA Covid-19 vaccine. *N. Engl. J. Med.* **383**, 2603–2615 (2020).
4. Sadoff, J. et al. Final analysis of efficacy and safety of single-dose Ad26.COV2.S. *N. Engl. J. Med.* **386**, 847–860 (2022).
5. Voysey, M. et al. Safety and efficacy of the ChAdOx1 nCoV-19 vaccine (AZD1222) against SARS-CoV-2: an interim analysis of four randomised controlled trials in Brazil, South Africa, and the UK. *Lancet* **397**, 99–111 (2021).
6. Tseng, H. F. et al. Effectiveness of mRNA-1273 against SARS-CoV-2 Omicron and Delta variants. *Nat. Med.* **28**, 1063–1071 (2022).
7. Muik, A. et al. Neutralization of SARS-CoV-2 Omicron by BNT162b2 mRNA vaccine–elicited human sera. *Science* **375**, 678–680 (2022).
8. Wang, Y. et al. Scalable live-attenuated SARS-CoV-2 vaccine candidate demonstrates preclinical safety and efficacy. *Proc. Natl Acad. Sci. USA* **118**, e2102775118, https://doi.org/10.1073/pnas.2102775118 (2021).
9. Nouailles, G. et al. Live-attenuated vaccine sCPD9 elicits superior mucosal and systemic immunity to SARS-CoV-2 variants in hamsters. *Nat. Microbiol.* **8**, 860–874, https://doi.org/10.1038/s41564-023-01352-8 (2023).
10. Stauft, C. B. et al. Intranasal or airborne transmission-mediated delivery of an attenuated SARS-CoV-2 protects Syrian hamsters against new variants. *Nat. Commun.* **14**, 3393 (2023).
11. Afkhami, S. et al. Respiratory mucosal delivery of next-generation COVID-19 vaccine provides robust protection against both ancestral and variant strains of SARS-CoV-2. *Cell* **185**, 896–915.e819 (2022).
12. Minor, P. D. The molecular biology of poliovaccines. *J. Gen. Virol.* **73**, 3065–3077 (1992).
13. Platt, L. R., Estivariz, C. F. & Sutter, R. W. Vaccine-associated paralytic poliomyelitis: a review of the epidemiology and estimation of the global burden. *J. Infect. Dis.* **210**, S380–S389 (2014).
14. Almazan, F. et al. Engineering a replication-competent, propagation-defective Middle East respiratory syndrome coronavirus as a vaccine candidate. *mBio* **4**, e00650–00613 (2013).
15. Gutierrez-Alvarez, J. et al. Middle East respiratory syndrome coronavirus vaccine based on a propagation-defective RNA replicon elicited sterilizing immunity in mice. *Proc. Natl Acad. Sci. USA* **118**, e2111075118, https://doi.org/10.1073/pnas.2111075118 (2021).
16. Zhang, X. et al. A trans-complementation system for SARS-CoV-2 recapitulates authentic viral replication without virulence. *Cell* **184**, 2229–2238.e2213 (2021).
17. Netland, J. et al. Immunization with an attenuated severe acute respiratory syndrome coronavirus deleted in E protein protects against lethal respiratory disease. *Virology* **399**, 120–128 (2010).
18. Grifoni, A. et al. Targets of T cell responses to SARS-CoV-2 Coronavirus in humans with COVID-19 disease and unexposed individuals. *Cell* **181**, 1489–1501.e1415 (2020).
19. Peng, Y. et al. Broad and strong memory CD4+ and CD8+ T cells induced by SARS-CoV-2 in UK convalescent individuals following COVID-19. *Nat. Immunol.* **21**, 1336–1345 (2020).
20. Yoo, J. S. et al. SARS-CoV-2 inhibits induction of the MHC class I pathway by targeting the STAT1-IRF1-NLRC5 axis. *Nat. Commun.* **12**, 6602 (2021).
21. Kimura, I. et al. Sarbecovirus ORF6 proteins hamper induction of interferon signaling. *Cell Rep.* **34**, 108916 (2021).
22. Zhang, Y. et al. The ORF8 protein of SARS-CoV-2 mediates immune evasion through down-regulating MHC-Iota. *Proc. Natl Acad. Sci. USA* **118**, e2024202118, https://doi.org/10.1073/pnas.2024202118 (2021).
23. Wagner, C. et al. Positive selection underlies repeated knockout of ORF8 in SARS-CoV-2 evolution. *Nat. Commun.* **15**, 3207 (2024).
24. Liu, Y. et al. A live-attenuated SARS-CoV-2 vaccine candidate with accessory protein deletions. *Nat. Commun.* **13**, 4337 (2022).
25. Silvas, J. A. et al. Contribution of SARS-CoV-2 accessory proteins to viral pathogenicity in K18 human ACE2 transgenic mice. *J. Virol.* **95**, e0040221 (2021).

26. Melade, J. et al. A simple reverse genetics method to generate recombinant coronaviruses. *EMBO Rep.* **23**, e53820 (2022).
27. Kipfer, E. T. et al. Rapid cloning-free mutagenesis of new SARS-CoV-2 variants using a novel reverse genetics platform. *eLife* **12**, RP89035 (2023).
28. Cattin-Ortola, J. et al. Sequences in the cytoplasmic tail of SARS-CoV-2 Spike facilitate expression at the cell surface and syncytia formation. *Nat. Commun.* **12**, 5333 (2021).
29. Chen, I. P. et al. Viral E protein neutralizes BET protein-mediated post-entry antagonism of SARS-CoV-2. *Cell Rep.* **40**, 111088 (2022).
30. Vann, K. R. et al. Binding of the SARS-CoV-2 envelope E protein to human BRD4 is essential for infection. *Structure* **30**, 1224–1232.e1225 (2022).
31. Hadfield, J. et al. Nextstrain: real-time tracking of pathogen evolution. https://nextstrain.org/ncov/gisaid/global/all-time?c=gt-ORF8_8&l=radial (2018).
32. Sia, S. F. et al. Pathogenesis and transmission of SARS-CoV-2 in golden hamsters. *Nature* **583**, 834–838 (2020).
33. Ulrich, L. et al. Enhanced fitness of SARS-CoV-2 variant of concern Alpha but not Beta. *Nature* **602**, 307–313 (2022).
34. Corman, V. M. et al. Detection of 2019 novel coronavirus (2019-nCoV) by real-time RT-PCR. *Eurosurveillance* **25**, 2000045, https://doi.org/10.2807/1560-7917.ES.2020.25.3.2000045 (2020).
35. Yu, X., Fournier, S., Allison, J. P., Sharpe, A. H. & Hodes, R. J. The role of B7 costimulation in CD4/CD8 T cell homeostasis. *J. Immunol.* **164**, 3543–3553 (2000).
36. Wong, S. C., Oh, E., Ng, C. H. & Lam, K. P. Impaired germinal center formation and recall T-cell-dependent immune responses in mice lacking the costimulatory ligand B7-H2. *Blood* **102**, 1381–1388 (2003).
37. Roussel, L. & Vinh, D. C. ICOSL in host defense at epithelial barriers: lessons from ICOSLG deficiency. *Curr. Opin. Immunol.* **72**, 21–26 (2021).
38. Jung, J. et al. Transmission and infectious SARS-CoV-2 shedding kinetics in vaccinated and unvaccinated individuals. *JAMA Netw. Open* **5**, e2213606 (2022).
39. Martinez-Baz, I. et al. Effect of COVID-19 vaccination on the SARS-CoV-2 transmission among social and household close contacts: a cohort study. *J. Infect. Public Health* **16**, 410–417 (2023).
40. Miteva, D. et al. Mucosal COVID-19 vaccines: risks, benefits and control of the pandemic. *World J. Virol.* **11**, 221–236 (2022).
41. Singanayagam, A. et al. Community transmission and viral load kinetics of the SARS-CoV-2 delta (B.1.617.2) variant in vaccinated and unvaccinated individuals in the UK: a prospective, longitudinal, cohort study. *Lancet Infect. Dis.* **22**, 183–195 (2022).
42. Mongin, D. et al. Effect of SARS-CoV-2 prior infection and mRNA vaccination on contagiousness and susceptibility to infection. *Nat. Commun.* **14**, 5452 (2023).
43. Thi Nhu Thao, T. et al. Rapid reconstruction of SARS-CoV-2 using a synthetic genomics platform. *Nature* **582**, 561–565 (2020).
44. Chu, D. K. W. et al. Molecular diagnosis of a novel coronavirus (2019-nCoV) causing an outbreak of pneumonia. *Clin. Chem.* **66**, 549–555 (2020).
45. Bankhead, P. et al. QuPath: open source software for digital pathology image analysis. *Sci. Rep.* **7**, 16878 (2017).
46. Protocol: Real-time RT-PCR assays for the detection of SARS-CoV-2 Institut Pasteur, Paris.
47. Wernike, K. et al. Multi-species ELISA for the detection of antibodies against SARS-CoV-2 in animals. *Transbound. Emerg. Dis.* **68**, 1779–1785 (2021).
48. Stegmann, K. M. et al. Inhibitors of dihydroorotate dehydrogenase cooperate with molnupiravir and N4-hydroxycytidine to suppress SARS-CoV-2 replication. *iScience* **25**, 104293 (2022).
49. Breithaupt, A., Sick, F., Golender, N., Beer, M. & Wernike, K. Characterization of experimental Shuni virus infection in the mouse. *Vet. Pathol.* **60**, 341–351 (2023).
50. Bussmann, B. M., Reiche, S., Jacob, L. H., Braun, J. M. & Jassoy, C. Antigenic and cellular localisation analysis of the severe acute respiratory syndrome coronavirus nucleocapsid protein using monoclonal antibodies. *Virus Res.* **122**, 119–126 (2006).
51. Rihn, S. J. et al. A plasmid DNA-launched SARS-CoV-2 reverse genetics system and coronavirus toolkit for COVID-19 research. *PLoS Biol.* **19**, e3001091 (2021).
52. Miyamoto, Y. et al. SARS-CoV-2 ORF6 disrupts nucleocytoplasmic trafficking to advance viral replication. *Commun. Biol.* **5**, 483 (2022).

Acknowledgements

We are grateful to Laurent Perez and Christian Münz for helpful comments on the manuscript. The authors thank the BioEM lab and Mohamed Chami of the Biozentrum, University of Basel, CH, for their support with electron microscopy and the DBM Microscopy Core Facility for support with image acquisition and analysis. We thank Sven Reiche (FLI, Greifswald, GER) for the generous provision of monoclonal anti-S and anti-N antibodies, which were obtained through the EU H2020 project EVA-GLOBAL, project #871029, and Yoichi Miyamoto (Natl. Inst. Biomed. Innovation, Health and Nutrition, Osaka, J) for the anti-ORF6 antibody. We are thankful to Mareen Grawe, Robin Brandt, and the animal caretakers at FLI for their essential help. We thank G. Kochs, Freiburg, GER, and the Bundeswehr Institute of Microbiology, Munich, GER for providing the SARS-CoV-2 Wuhan isolates and Martin Daeumer, Alex Thielen (Seq-It GmbH, Kaiserslautern, GER) and Adrian Egli & team (USB, Basel, CH) for expert NGS support. pCMVR8.74 and pMD2.G were a gift from Didier Trono (RRID: Addgene_12259), pLEX307-TMPRSS2-blast was a gift from Alejandro Chavez & Sho Iketani (RRID: Addgene_158458). pHR_PGK-hACE2 was a gift from Brad Rosenberg (RRID: Addgene_161612). Vero E6 cells and synthetic SARS-CoV-2 virus (Wuhan-1, GenBank No. MT108784) were kindly provided by Volker Thiel. Graphical symbols in Figs. 3 and 5 and Supplementary Figs. 1 and 2 were created with BioRender.com. This research was co-funded through a federal project grant through the Innosuisse project #52533.1 IP-LS and by RocketVax AG, Basel, CH, through a project grant with the University Hospital Basel/Canton Basel Stadt, CH, granted to TK. The funders had no influence on the experimental design or conduct of work.

Author contributions

This work was conceived by M.J.L., F.O., D.H., V.C., M.B., C.M., and T.K., experimental procedures were performed by M.J.L, F.O., D.H., J.S., E.K., N.J.H., J.K, B.C, L.U., Y.Z., L.U., D.Ho., A.B., T.B., and C.L., data analysis was conducted by M.J.L., F.O., D.H., A.B., T.B., and J.S. The manuscript was jointly written by M.J.L, F.O., D.H., and T.K., with editing provided by J.S., D.Ho., M.B. and C.M. M.J.L, F.O., and D.H. share co-first authorship and contributed equally to this work. All authors have read and approved the final version of the manuscript.

Competing interests

V.C. owns shares of RocketVax AG, Basel, CH. The other authors declare no competing interests. A patent application (no. WO 203/036947 A1) has been filed on the topic of this vaccine.

Additional information

Supplementary information The online version contains supplementary material available at https://doi.org/10.1038/s41541-024-00992-z.

Correspondence and requests for materials should be addressed to Thomas Klimkait.